# Sr Isotope Zoning in Plagioclase from Parinacota Volcano (Northern Chile): Quantifying Magma Mixing and Crustal Contamination

## C. GINIBRE[1,2]* AND J. P DAVIDSON[1]

[1]DEPARTMENT OF EARTH SCIENCES, DURHAM UNIVERSITY, SOUTH ROAD, DURHAM DH1 3LE, UK
[2]DEPARTEMENT DE MINERALOGIE, UNIVERSITE DE GENEVE, 13 RUE DES MARAICHERS, 1205 GENEVE, SWITZERLAND

*We present analyses of Sr isotope zoning by microdrilling and thermal ionization mass spectrometry in plagioclase crystals from Parinacota volcano (Central Volcanic Zone, northern Chile), which were analysed for major and minor element zoning in a previous study. Although the isotopic range of the bulk-rock samples is small at this volcano (0·7067–0·7070, except for one flow of mafic andesite at 0·7061), significant variations are seen (0·70649–0·70700) within and between plagioclase crystals. A general negative correlation is observed between Sr isotope composition and Sr concentration in the liquid in equilibrium with each plagioclase zone, as calculated from chemical zoning data and partition coefficients. Additional scatter is superimposed on this general trend, indicating a decoupling between isotopic and chemical variations for Sr. In one dacite sample a detailed isotopic profile shows increasing contamination during crystal growth, except for an abrupt decrease correlated with a dissolution surface and interpreted as a recharge event. We apply energy-constrained recharge, assimilation and fractional crystallization modelling to the melt evolution recorded in the chemical and isotopic zoning in this crystal. Results suggest 20% assimilation of the local wall-rock gneiss, at high initial temperatures. The isotopic data confirm the involvement of two contrasting mafic magmas, which are sampled at flank cinder cone vents. One (Lower Ajata) has a low Sr content with high [87]Sr/[86]Sr, the other (Upper Ajata) has a high Sr content with lower [87]Sr/[86]Sr. In some samples from Parinacota, the isotopic composition of plagioclase crystal rims or groundmass crystals is significantly higher than that of the high [87]Sr/[86]Sr mafic magma. In others, where chemical zoning profiles suggest that recharge was from the low [87]Sr/[86]Sr magma, the [87]Sr/[86]Sr of the groundmass and crystal rims is higher than expected. This indicates either additional parent magmas to the two previously identified, or further crustal assimilation, either at lower crustal*

*depths, before crystallization of plagioclase, or just after the last recharge. Our results illustrate the complexity of magma–crust interaction beneath Parinacota, which is likely to be representative of many other Central Andean volcanoes formed on thick crust. Such complex interactions can be revealed by combined study of chemical and isotopic zoning in plagioclase (in a textural petrographic context), despite a small whole-rock isotopic range. The distinct contamination patterns of various samples suggest an important role for the geometry, location and evolution of the magma plumbing system and, in general, variations of the thermal and compositional structure of the crust underneath the volcano.*

## INTRODUCTION

The influence of the various components (mantle wedge, lithospheric mantle, slab melt or fluids and continental crust) in the sources of arc magmatism is a subject of considerable debate and clearly varies between arcs. The role of lower continental crust in modifying magma compositions has been shown to be important all along the Andean volcanic arc (e.g. Hildreth & Moorbath, 1988; Wörner *et al.*, 1992; Davidson & de Silva, 1995; Garrison *et al.*, 2006). The Andean Central Volcanic Zone (CVZ) represents a segment of the continental arc where the crust is thickest; therefore, the chemical and isotopic characteristics of the magmas are expected to be strongly influenced by the nature of the crust beneath the volcanic

*Corresponding author. E-mail: catherine.ginibre@unige.ch

front. Several studies document the effect of this thick crust (Harmon *et al.*, 1984; Davidson *et al.*, 1991; Wörner *et al.*, 1994) and identify a difference in crustal composition in different domains in the lower crust [e.g. north and south of the Pica Gap, 19–21°S (Wörner *et al.*, 1994); the Arequipa Domain, to the north, is isotopically distinct from the domains to the south (Mamani *et al.*, 2008)]. McMillan *et al.* (1993) have also identified a relationship between the modification of crustal signature and the timing of crustal thickening.

A lower crust signature is particularly clear in the Nevados de Payachata volcanic region, located in northern Chile (18°S), next to the Bolivian border, including the Pleistocene to Holocene twin composite volcanoes Pomerape and Parinacota (Wörner *et al.*, 1988; Davidson *et al.*, 1990; McMillan *et al.*, 1993). The eruption products of the Parinacota stratovolcano are mainly andesitic and range from basaltic andesite to rhyodacite; most Parinacota samples have only moderately elevated Sr concentrations (900–1200 ppm) similar to other volcanic centres of the northern CVZ. However, two basaltic andesite units from recent flank eruptions (Ajata Flows) have contrasting concentrations of Sr (up to 1800 ppm vs 800 ppm) and other incompatible trace elements. These probably reflect different amounts of crustal assimilation at different depths, the high incompatible element contents being typical of a lower crustal signature. The study of the relationships between such mafic magmas and the products of the main edifice is therefore a way in which to investigate magma–crust interactions beneath this volcano. The influence of mixing with two mafic end-member magmas during the whole history of Parinacota has been implied by Bourdon *et al.* (2000) based on U–Th data. Ginibre & Wörner (2007) showed, based on trace element zoning in plagioclase, that such mixing occurred with alternating magma recharge events of increasing frequency through time. However, these studies do not allow detailed identification of crustal assimilation. For that purpose, we have examined Sr isotopic zoning in plagioclase at high spatial resolution. The way in which two mafic magmas interact with the crust, and are modified by processes such as fractional crystallization and assimilation, will depend on the details of the plumbing system (magma chamber size, location and interconnectivity) as well as the nature of the crust. This study thus allows us to make further inferences about the magma plumbing system of Parinacota Volcano.

Sr isotope microsampling has been used previously to elucidate disequilibrium and mixing in magmatic systems (e.g. Davidson & Tepley, 1997; Tepley *et al.*, 1999, 2000; Davidson *et al.*, 2007). In general, progressive contamination of a magma by crustal assimilation causes the $^{87}Sr/^{86}Sr$ ratio to increase, whereas recharge by more mafic and generally less contaminated magma decreases the $^{87}Sr/^{86}Sr$ ratio. The case of Parinacota is more complex: the two recent mafic magmas (the Ajata Flows) identified as possible recharge end-members (Ginibre & Wörner, 2007) not only have contrasting trace element contents, they also have distinct Sr isotopic compositions ($^{87}Sr/^{86}Sr = 0.7067$ and $0.7061$). Therefore, changes in $^{87}Sr/^{86}Sr$ depend not only on the recharge and contamination rates, but also on the nature of the mafic recharge magma, which can have either lower or higher $^{87}Sr/^{86}Sr$ than the resident magma. In combination with chemical zoning (Ginibre & Wörner, 2007), the core–rim isotopic variations of feldspars can be used to reconstruct the evolutionary histories of the magmas from which they grew.

Our study focuses on two issues: (1) the diversity of magmatic processes at a single volcano, which is best seen by comparing a selection of different samples; (2) quantification of the assimilation process. The latter has been analyzed and modelled in particular detail for one sample where the size of the zones allows recovery of an extensive record.

## BACKGROUND STUDIES OF PARINACOTA VOLCANO
### Stratigraphy

The stratigraphy of Parinacota Volcano has been described by Wörner *et al.* (1988) and Hora *et al.* (2007), and is summarized in Fig. 1. An early Chungara andesite is overlain by a plateau of Rhyolite Domes [stage I b of Wörner *et al.* (1988), but included in the Old Cone by Hora *et al.* (2007, 2009)]. The main stratocone, referred to as the Old Cone, consists of lavas ranging from basaltic andesite to rhyodacite, most of them amphibole-bearing. The Old Cone was subsequently partly removed by a sector collapse at about 15–18 ka, although this age has been debated by Wörner *et al.* (2000), Clavero *et al.* (2002, 2004), Hora *et al.* (2007) and Sáez *et al.* (2007). After collapse, the cone was rebuilt to its current height with more homogeneous andesite, referred to as Healing Flows. The last stage, the Ajata Flows, comprises three distinct homogeneous groups of recent lavas from flank eruptions from a single fissure. The Lower Ajata Flows and the Upper Ajata Flows are almost aphyric basaltic andesites erupted from the same vent. The High Ajata Flows are slightly more evolved, plagioclase-phyric, more similar to Healing Flow samples, and erupted from a vent located higher along the fissure. For the present study, we selected samples to represent the stratigraphic range from the Old Cone stage to the Ajata Flows.

### Geochemistry

Parinacota lavas have typical high-K calc-alkaline compositions, with high concentrations of Sr, Ba and Ti compared with other CVZ volcanoes (Davidson *et al.*, 1990).
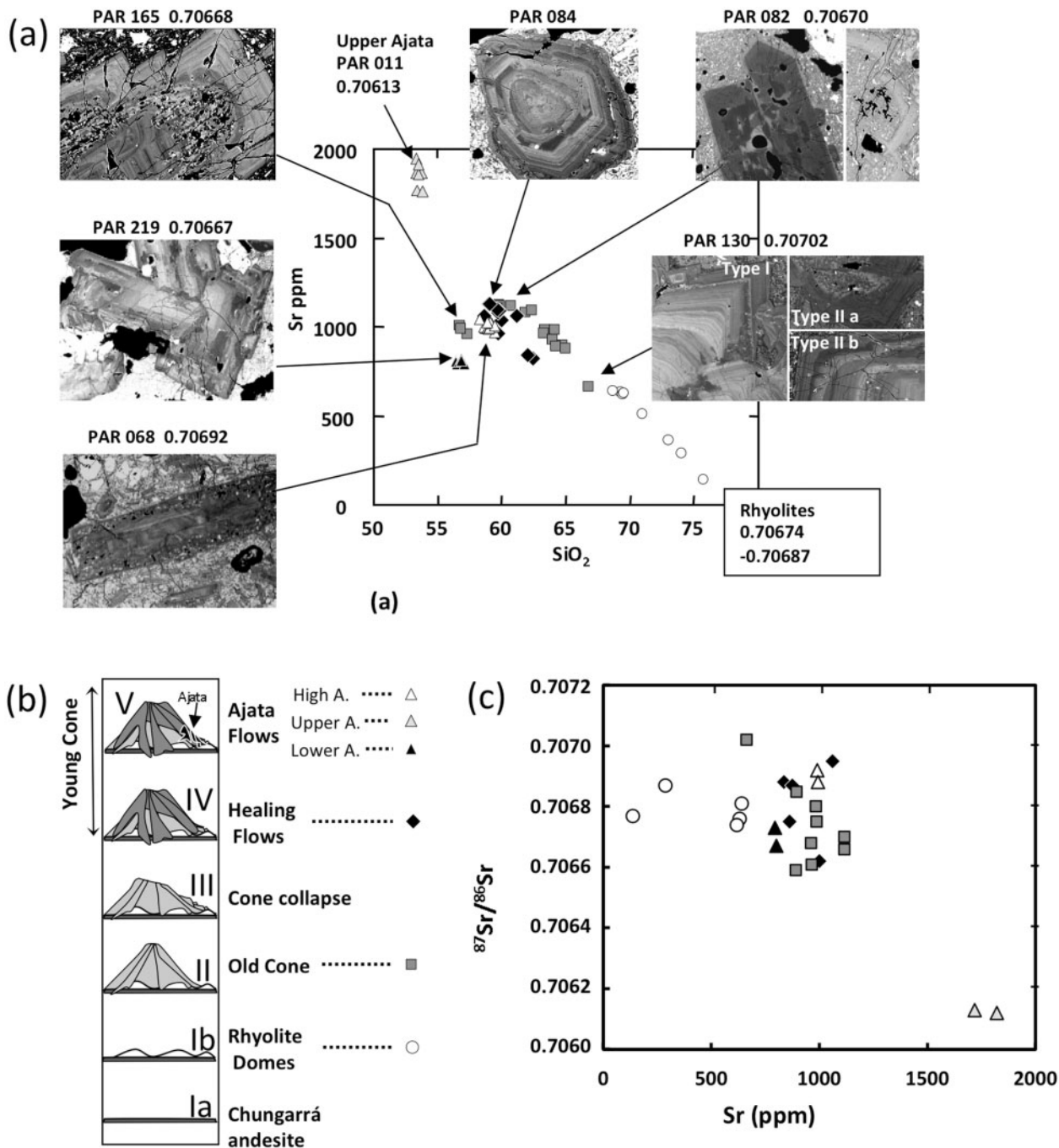
**Fig. 1.** (a) Sr (ppm) concentrations of Parinacota bulk-rock samples vs SiO$_2$ (wt %) (after Wörner *et al.*, 1988). Samples selected for this study are shown along with their bulk-rock Sr isotope ratios from Davidson *et al.* (1990) and images of plagioclase zoning (see text for the description of PAR 130 plagioclase types), except for PAR 11, which is plagioclase free. (b) Simplified stratigraphic evolution of Parinacota volcano showing the main units with the symbols used in (a) and (c). (c) Sr isotope composition vs Sr concentration for the same samples [data from Davidson *et al.* (1990)].

The stratigraphic subdivisions are reinforced by chemical distinctions among the main groups defined above (Fig. 1), which reflect different processes and/or parental magma inputs. The Lower Ajata Flows have low Sr and Ba contents (similar to other rocks from the CVZ) in contrast to extremely high Sr and Ba (both >1600 ppm) in the Upper Ajata Flows. All Parinacota samples fall between these two mafic magma types and the evolved end-members (rhyolites from stage Ib) in all element vs silica diagrams, as shown for Sr in Fig. 1. It has been suggested (McMillan

*et al.*, 1993) that the Ajata lavas are possibly not related to the main stratocone. However, U–Th data (Bourdon *et al.*, 2000; Hora *et al.*, 2009) and plagioclase chemical zoning (Ginibre & Wörner, 2007) strongly suggest that all Parinacota lava compositions derive from mixing between two types of mafic end-member, similar to the Upper and Lower Ajata, and a felsic end-member similar to the rhyolite domes, possibly accompanied by fractional crystallization.

Sr isotopic compositions in most Parinacota bulk-rock samples (Fig. 1) vary only between 0·70660 and 0·70702 (Davidson *et al.*, 1990). The Upper Ajata Flows (high Sr) have less radiogenic Sr (0·70613), whereas the other mafic end-member (Lower Ajata) has a $^{87}Sr/^{86}Sr$ of 0·70667–0·70673. The most radiogenic sample is an Old Cone dacite PAR 130 (0·70702), whereas the Rhyolite Domes (0·70676–0·70687) fall into the range of the more mafic samples (0·70665–0·70692; Upper Ajata not included).

## Samples and plagioclase zoning

The results of a previous study on chemical zoning of plagioclase crystals at Parinacota (Ginibre & Wörner, 2007) are essential to the interpretation of our new isotopic microsampling data. For this reason, the previously published data are shown alongside the microsampling zones and isotopic results of our current study in Figs 2–4. To provide the context for our integrated data and consequent interpretations we first summarize the main interpretations of Ginibre & Wörner (2007).

The samples studied are from the suites of Wörner *et al.* (1988), Davidson *et al.* (1990), and Entemann (1994). Where possible we indicate the correspondence to the units analysed by Hora *et al.* (2007, 2009). Samples were selected from each stratigraphic unit to be as representative as possible in terms of chemistry, petrography and plagioclase zoning patterns. Chemical zoning in plagioclase within a given sample generally consists of a few zoning types, and in each type zoning is consistent between crystals. Backscattered electron (BSE) images and Sr–Fe diagrams are shown in Fig. 2 (Old Cone), Fig. 3 (Healing Flows) and Fig. 4 (Ajata Flows).

### Old Cone (OC)

Samples were divided into three groups (OC1–3) on the basis of chemistry and petrography, and one sample from each group was chosen. The main group [Group OC1 of Ginibre & Wörner (2007)] consists of andesitic to dacitic lavas with abundant evidence for magma mixing (see below). Most Old Cone lavas analysed by Hora *et al.* (2009) seem to fall into this group, including PAR 082 (their unit oc2) and the Border Dacite (their unit ocb). In all variation diagrams against $SiO_2$, OC1 samples lie on a mixing line between rhyolites and a mafic end-member compositionally close to the Upper Ajata. Together with their mineralogy, this suggests that the andesites and

dacites reflect mixing of evolved magmas with variable amounts of high-Sr, feldspar-free basaltic andesite.

PAR 082, dated by Hora *et al.* (2007) at 20 ka, is a representative amphibole–two-pyroxene andesite of the OC1 group. Plagioclase-free clusters of amphibole and pyroxene with olivine cores are common. Plagioclase is present as scarce, isolated, often large (up to 1 cm) crystals with a sodic inner part ($An_{25-50}$; zone 2 in Fig. 2a), with low Fe and Mg (1500–2000 ppm and <100 ppm respectively) and variable Sr (1000–3200 ppm; the lower values being more common), and a fine, sieve-textured calcic rim ($An_{55-65}$; zone 1 in Fig. 2a) with high Fe, Mg (>4500 ppm and >300 ppm respectively) and Sr (3000–4500 ppm) similar to the groundmass crystals (GmC in Fig. 2a). Sanidine crystals with sieve-textured rims and sodic plagioclase inclusions are also present. All feldspar crystals are interpreted as antecrysts, being inherited from a rhyodacitic magma or crystal mush, possibly from the underlying rhyolite domes or a contemporaneous, similar, non-erupted magma, by mixing with a Sr-rich mafic end-member, as suggested above. This may occur either by magma mixing (basaltic andesite–rhyolite) or by remobilization of partially solidified felsic cumulate by an andesitic magma, although the absence of feldspar clusters, which might be expected from a disaggregated cumulate, makes the magma mixing hypothesis more likely.

Group OC2 is more homogeneous in composition and texture, and consists of basaltic andesites from the NW flank. These lavas were apparently not analysed by Hora *et al.* (2007, 2009) as none of their Old Cone samples have such a mafic composition. Sr and Ba concentrations are lower than in the Old Cone andesites, but higher than in the Lower Ajata Flows. PAR 165 is representative of this group and contains abundant plagioclase, orthopyroxene and clinopyroxene in clusters containing few reacted olivine crystals and rare, entirely oxidized amphiboles. Plagioclase phenocrysts in PAR 165 are characterized by a relatively sodic core ($An_{35-50}$; zone 1 in Fig. 2b) separated from the outer more calcic zone ($An_{45-65}$; zone 3 in Fig. 2b) by a resorption zone of variable extent (zone 2 in Fig. 2b). Resorption zones and outer zones are richer in Ca, Fe, Mg and Ti, and poorer in Sr than the core, which is interpreted as reflecting a mafic recharge event by a Sr-poor magma. Groundmass crystals (not shown in Fig. 2b) are similar to the outer zone, except for a higher Fe content up to 6500 ppm, which is interpreted as a 'rim effect' owing to a combination of analytical artefact (X-ray secondary fluorescence), kinetic effects caused by rapid growth and possible changes in $fO_2$ [see Ginibre & Wörner (2007) for a discussion]. This suggests that there was no magma mixing immediately before eruption, contrasting with most of the other samples.

PAR 130, representing group OC3, is from a dacite dome on the north flank of the volcano, and is related spatially
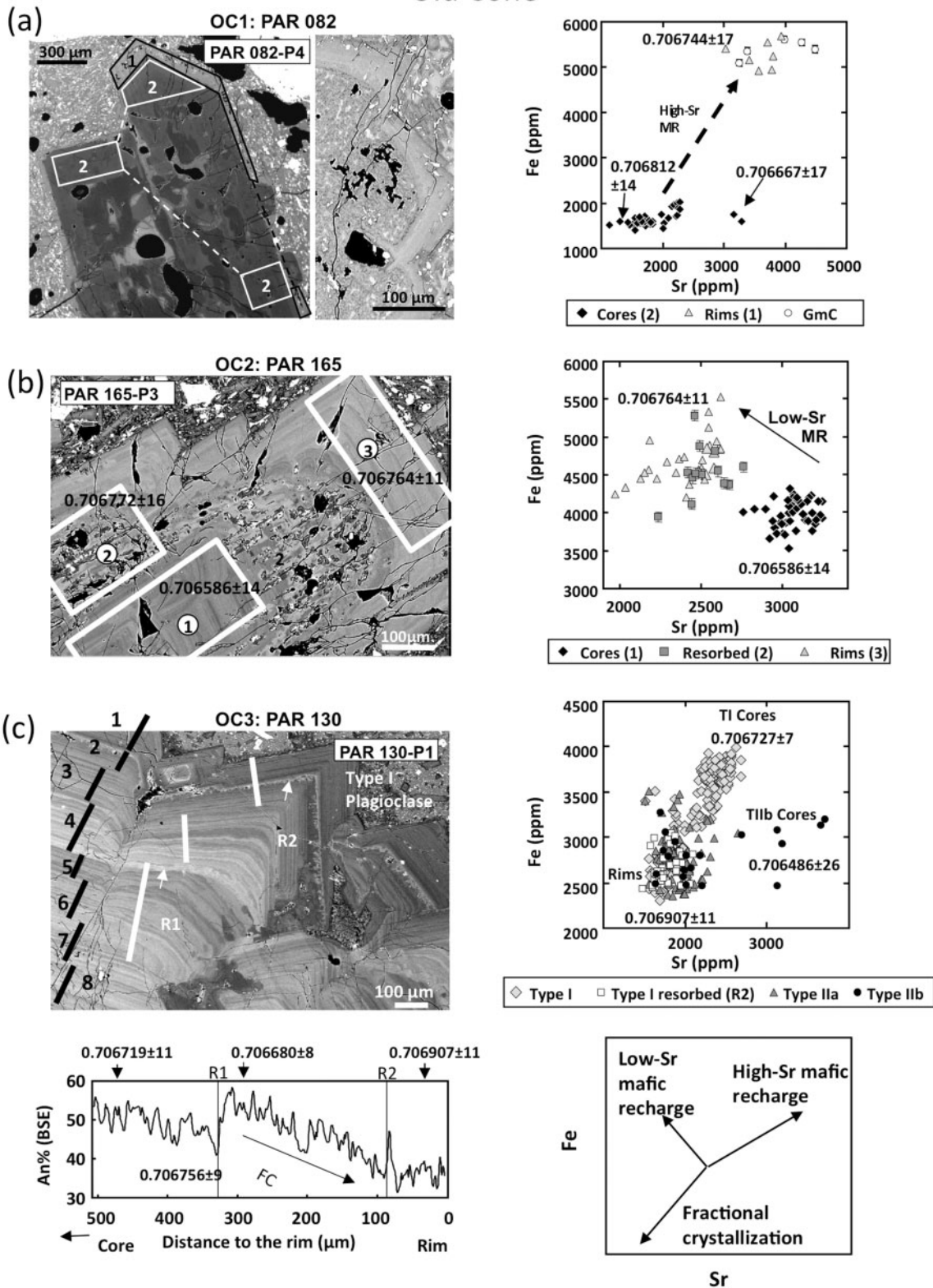
**Fig. 2.** Back-scattered electron (BSE) images of representative drilled crystals and Sr and Fe concentrations of all crystals analysed showing the main interpretations of the chemical data (Ginibre & Wörner, 2007) for Old Cone samples. Representative $^{87}Sr/^{86}Sr$ values from drilled zones

(continued)

to unit ocl of Hora *et al.* (2009). This dome was not analysed by those researchers, and has a significantly higher Sr isotope ratio (0·70702; Davidson *et al.*, 1990) than the OCl samples. No clear petrographic evidence for magma mixing is seen. The mineral assemblage includes abundant plagioclase, two pyroxenes, rare small amphiboles and rounded biotites. OC3 plagioclase crystals are mainly oscillatory zoned, with occasional resorption surfaces (Fig. 2c). Several types of zoning have been defined in OC3 (Ginibre *et al.*, 2002): Type I crystals are large and oscillatory zoned with decreasing Fe, Sr and An from core to rim reflecting fractional crystallization. Other smaller crystals (Type II) show more significant dissolution in the core (Fig. 1a) with low Fe at high An and variable Sr (Type IIa, finely patchy zoned core, low-Sr; Type IIb, evident dissolution surfaces, high-Sr core). The chemical zoning in this sample was interpreted to reflect near closed-system crystallization. A possible subtle mixing event with a more mafic magma, either by self-mixing in a weakly zoned magma chamber or by recharge from a different reservoir, was identified rimward of the resorption surface R1 in Type I crystals (with increased An, Sr and Fe). The influence of an $H_2O$-rich, more differentiated magma is suggested at the end of crystallization (resorption surface R2 in Type I crystals and cores of Type IIa crystals such as P9), by the increased An content without clear changes in Fe and Sr and a decreased Ba content in the absence of crystallizing sanidine or biotite. This has been interpreted as an increased influence of the magma chamber margin (Ginibre *et al.*, 2002). High-Sr Type IIb cores are thought to be inherited from high-Sr dominated earlier stages, possibly brought by a high-Sr recharge magma.

### Young Cone (Healing Flows)

Healing Flow samples all have similar compositions and can be divided petrographically into two groups: Group I (PAR 084) has large (2–3 mm) abundant plagioclase, whereas plagioclase crystals are smaller and less abundant in Group II (Ginibre & Wörner, 2007), which was not analysed in the present study. In addition to plagioclase, PAR 084 includes two pyroxenes, oxides and apatite, and rare, small, oxidized pseudomorphs after amphibole. Plagioclase crystals ($An_{35-65}$) are characterized by numerous, more or less rounded, concentric resorption surfaces, commonly associated with concentric patchy zoning and large crystallized melt inclusions. Fe and Mg concentrations increase overall from cores to rims. All plagioclase crystals have two to three zones (from core to rim) defined by their Sr concentrations: high-Sr cores, a lower-Sr intermediate zone and high-Sr rims. This zoning is interpreted as evidence for alternating recharge with two mafic magmas, one with low Sr (similar to the Lower Ajata magma), the other one with high Sr (similar to the Upper Ajata magma).

### Ajata Flows

Among the three types of Ajata Flows, the Upper Ajata group consists of basaltic andesites without any plagioclase phenocrysts. Its chemical and isotopic composition makes it a possible end-member. The mineral assemblage is characterized by phenocrysts of subhedral olivine, commonly with small spinel inclusions, rare microphenocrysts of augite, titanomagnetite and plagioclase, and traces of highly oxidized amphibole.

High Ajata flows (sample PAR 068) consist of mafic andesites more similar to Healing Flow samples and contain many resorbed plagioclase phenocrysts, clinopyroxene and rare orthopyroxene, both with large apatite inclusions, Fe–Ti oxides, sparse olivine cores with pyroxene and Fe–Ti oxide reaction rims, and sparse rounded amphiboles with oxidized rims. Plagioclase zoning shows an extensive patchy zone surrounding, in many cases, distinct unzoned or normally zoned cores, and in turn surrounded by narrow (50 μm) oscillatory zoned rims (Fig. 4b). The patchy zone includes large glass inclusions and, in some crystals, several internal discontinuities, interpreted as dissolution surfaces. The major element zoning patterns, combined with large Sr concentration variations among crystal cores, interpreted as inherited from both low-Sr and high-Sr magma, are consistent with multiple mafic recharge events. Intermediate to low Sr contents in the resorption zone and rims suggest that the recharge events occurred with relatively low-Sr magma or with rapid alternation of low- and high-Sr magmas.

The Lower Ajata Flow contains few large (up to 7 mm) resorbed plagioclase crystals. Sample PAR 2l9 is one of these (Fig. 4a). This sample shows evidence for magma mixing. It contains numerous skeletal olivines in the matrix and some olivine phenocrysts with skeletal overgrowths; 1–7 mm resorbed plagioclase occurs either isolated or in clusters together with clinopyroxene, small

**Fig. 2.** Continued

(numbered on the BSE images) are shown on subsequent diagrams (the complete dataset is shown in Fig. 5). The general effect of recharge events and fractional crystallization on Fe and Sr concentrations is shown schematically in the bottom right-hand panel; it should be noted that the trends of fractional crystallization and mixing with high-Sr recharge on Sr concentrations are similar, illustrating the potential of our new isotopic data to distinguish petrogenetic processes. (a) PAR 082-P4 and detail of a sieve-textured crystal. GmC, groundmass crystals; MR, mafic recharge. (b) PAR 165-P3. (c) PAR l30-Pl. In (c) black bars on the BSE image represent the width of each microdrilled zone (parallel to the crystal outline); white lines indicate the location of the BSE-based An profile shown in the panel below. R1 and R2, resorption surfaces; FC, fractional crystallization.
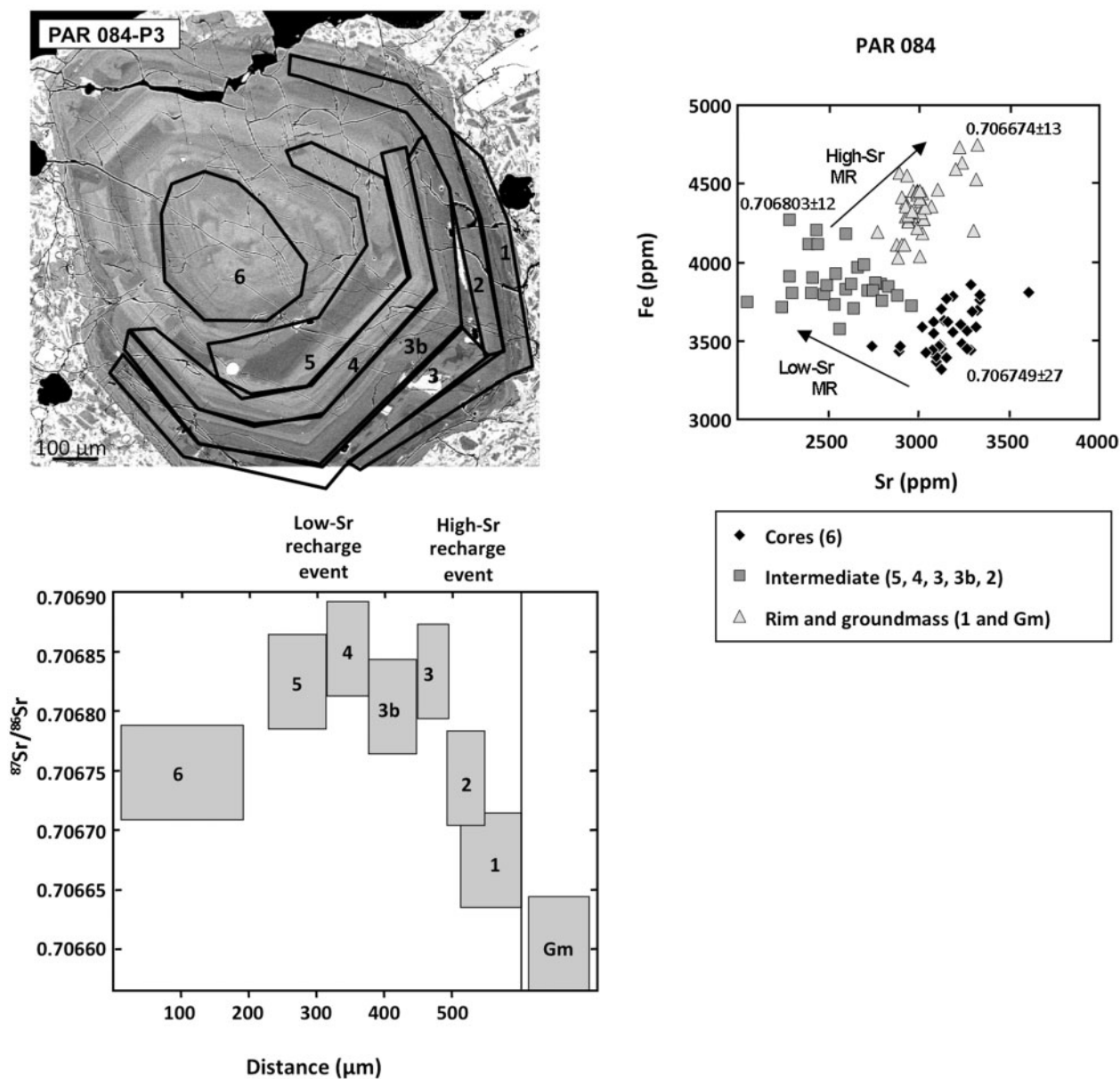
## Healing Flows



**Fig. 3.** BSE image, chemical and isotopic data for Healing Flow sample (PAR 084). Processes inferred from chemical zoning are shown in the Fe–Sr diagram (MR, mafic recharge). For the core, intermediate and rim zones shown in the Fe–Sr diagram, the drilled zone numbers, as shown in the BSE image and in the $^{87}Sr/^{86}Sr$ profile, are indicated.

oxidized pseudomorphs of amphibole and Fe–Ti oxides. Plagioclase zoning includes calcic cores with high Sr concentration, and an extensive resorption zone with lower Sr, patchy zoning and glass inclusions, surrounded by a narrow (10 μm), highly calcic outer rim (An$_{60}$) with low Sr and very high Fe contents, similar to the groundmass crystals. All plagioclase crystals are interpreted as inherited crystals (antecrysts) from an earlier magmatic

event subsequently sampled by an aphyric low-Sr basaltic andesite.

## Sr ISOTOPE MICROSAMPLING
### Purpose and method

We used the same samples as those in the chemical zoning study of Ginibre & Wörner (2007), with the exception of
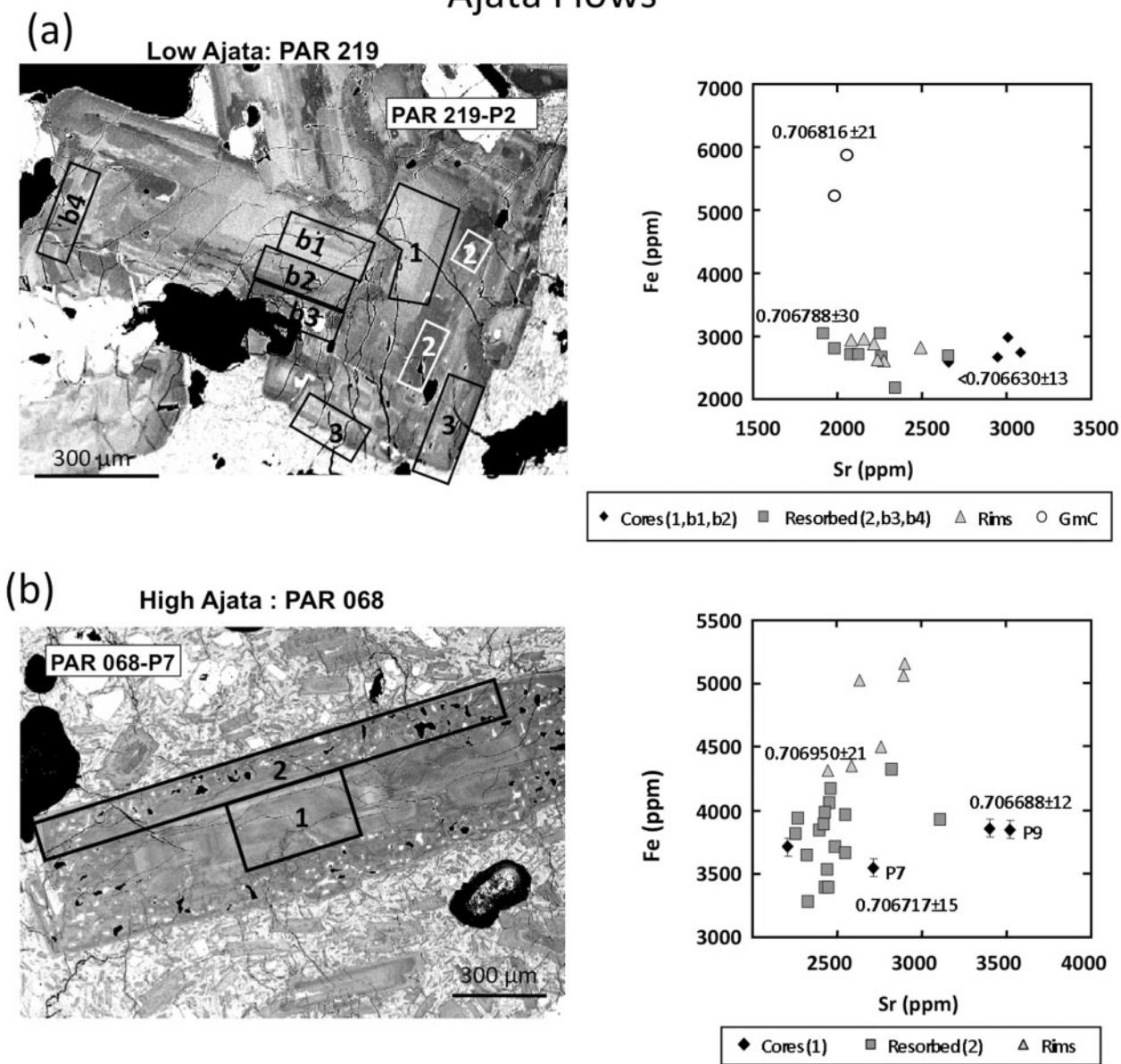
## Ajata Flows



**Fig. 4.** BSE image and Fe–Sr diagrams for Ajata samples. Upper Ajata is not shown because it lacks plagioclase phenocrysts. (a) PAR 219 (Lower Ajata). In this sample sieve-textured rims are too narrow to be drilled. (b) PAR 068 (High Ajata).

one Healing Flow sample, which we omitted from the current study. In each sample, a few crystals believed to be representative of crystal composition and zoning (one for each zoning type), were microdrilled and analysed, zone by zone, for Sr isotopes.

Ginibre & Wörner (2007) have shown, through chemical zoning in plagioclase, the occurrence of recharge events with mafic magmas of variable chemical composition at Parinacota. The high Sr and lower Sr concentrations seen following mafic recharge events in the stratigraphy of feldspar crystals suggest that the Upper Ajata and Lower Ajata magma types respectively may be the mafic mixing end-members. The contribution that this additional Sr isotope microsampling study makes is (1) validation of the end-member mixing roles of the Upper and Lower Ajata magma types, made possible as they have distinct Sr isotopic characteristics, and (2) an evaluation of the degree to which open-system processes (interaction with the crust) are involved. The detailed microsampling of one of the particularly spectacular large oscillatory zoned crystals from PAR 130 (OC3) also serves as a detailed case study, allowing us to track and quantify the process of crustal

assimilation during plagioclase crystallization archived in the core–rim record of the crystal.

## Analytical techniques

Feldspar crystals were microdrilled at the level of petrographically and chemically distinct growth zones at the Department of Earth Sciences, Durham University, using a New Wave Micromill[TM]. Sr chemical separation was performed on Sr-spec resin, and thermal ionization mass spectrometry (TIMS) analyses were carried out on a Thermo-Finnigan Triton[TM] using TaF activator on Re filaments. Details of the technique have been given by Charlier *et al.* (2006). All drilled samples were obtained on thin sections of 40–60 μm thickness. The depth of drilling was adjusted by trial and error on other crystals of the same thin section to avoid touching the underlying glass. In rare cases (e.g. PAR 219), however, the drilled sample was contaminated during drilling with the underlying glass, which has a low Sr concentration (5 ppm) but an isotopic ratio of 0·721404 ± 14. In these cases, the results are shown but their significance is discussed in the results sections.

Data were acquired during three periods of several weeks over 2 years and the long-term drift of the TIMS analysis was monitored with NBS987 on 3–12 ng standards. The average values and reproducibility (2σ) over the three periods are respectively 0·710252 ± 14, 0·710260 ± 14 and 0·710263 ± 14. Variations between these periods are taken into account by normalizing all the values to 0·710250. Total procedure blanks are usually below 50 pg and always below 100 pg, and the sizes of the drilled zones were adjusted, depending on Sr concentration, to contain more than 5 ng Sr (usually closer to 10 ng) so that the blank is below 1% of the analysed Sr sample. A few blank isotopic ratios were analysed and fall generally between 0·7090 and 0·7095, and in any case below 0·710. Therefore the blank contribution to variations of the isotopic ratios close to 0·7067 are around 0·000030 for 5 ng samples and 0·000015 for 10 ng samples, and we are therefore confident that the variations shown are real and exceed the ranges described by both error and blank. For each sample, square grids were drilled in the groundmass and, where possible, groundmass plagioclase crystals (above 10 crystals for each drilled sample) were also drilled and analysed. Because most Sr is in the plagioclase ($Kd_{Sr} \gg 1$), the analyses of groundmass crystals are typically more precise than those of the microlite-free groundmass, which is also more vulnerable to contamination.

Repeat analyses of the whole-rock [same samples as used by Davidson *et al.* (1990)] were carried out using the same technique as for the microdrilled samples but with 50 mg of whole-rock powder for dissolution and chemical separation, and running aliquots of *c.* 20 ng Sr on the TIMS system. Because of the young age of the lavas and low Rb/Sr ratio, age corrections are not significant and data are presented without them.

Microprobe data for Fe–Ti oxide thermometry were obtained at GZG Göttingen (Germany) on a JEOL JXA 8900RL electron microprobe using a 15 kv, 15 nA focused beam.

# RESULTS AND INTERPRETATION OF Sr MICROSAMPLING

## Whole-rock data

The new whole-rock Sr isotope analyses are within error of the previous ones except for sample PAR 130 and sample PAR 219 (Table 1). The significant but relatively small discrepancy for crystal-rich PAR 130 might be due to real sample heterogeneity or differences in the technique. The new value is obtained with the same method as used for the microdrilled samples and therefore should be more directly comparable. For PAR 219 the discrepancy between the two whole-rock isotopic ratios is probably due to the heterogeneity of the sample, because of the small number of large plagioclase grains having a lower $^{87}Sr/^{86}Sr$.

## Microdrilling data

The locations of drilled zones are shown on BSE images of the crystals before drilling and correspond to Sr isotopic ratios in Table 1 (see Figs 2–5). Isotopic profiles are shown only for large crystals (PAR 130 and PAR 084) in Figs 2 and 3 but other data are presented from core to rims for each crystal in Fig. 5. $^{87}Sr/^{86}Sr$ ratios are given with 2σ in-run error. However, the error bar on the drilled zones data in Fig. 5 takes into account the possible blank contribution. We present below the results and interpretations for each sample, with broader implications addressed in the discussion section.

Sr isotopic ratios of single zones versus the calculated Sr concentration of the melt in equilibrium with the plagioclase averaged for each drilled zone are shown in Fig. 6. Sr concentrations in the melt are calculated from Sr concentrations in the plagioclase [data from Ginibre & Wörner (2007)] and An content using the equation of Blundy & Wood (1991) and estimated crystallization temperatures. The reported uncertainty on Sr concentration in the melt (150 ppm) includes a term from the analytical uncertainty of the electron microprobe (120 ppm uncertainty in the analysis gives around 50 ppm on the calculated Sr melt), the effect of 50°C uncertainty on the temperature (50 ppm), and the effect of an uncertainty on the coefficients in the equation (50 ppm).

### *Old Cone*

In PAR 082, plagioclase cores range from very low Sr (1000 ppm) to relatively high Sr (3200 ppm) concentrations. Therefore we drilled the cores of several crystals

*Table 1: Sr concentrations and isotopic ratios of Parinacota whole-rock and microdrilled samples*

| Sample | Zone type | Analysis name | Sr Plag | Sr liq | $^{87}Sr/^{86}Sr_c$ | 2SE | Comments |
|---|---|---|---|---|---|---|---|
| *Ajata* | | | | | | | |
| PAR 219 | WR* | PAR219 | | 802 | 0·706670 | 0·00004 | |
| | WR2005 | PAR219 | | 802 | 0·706771 | 0·000008 | |
| | | PAR219P1-1 | 2022 | 469 | 0·706794 | 0·000017 | Glass contamination |
| | | PAR219P1-1b | 2022 | 469 | 0·706712 | 0·000017 | |
| | Resorbed rim | PAR219P1-2 | 2022 | 469 | 0·706784 | 0·000015 | Mixed with main zone? |
| | Core | PAR219P2-1 | 3080 | 1028 | 0·706630 | 0·000013 | Glass contamination |
| | Resorbed crystal | PAR219P2-2 | 2082 | 390 | 0·706711 | 0·000017 | Glass contamination |
| | | PAR219P2-3 | 2674 | 690 | 0·706765 | 0·000023 | Glass contamination |
| | | PAR219P2b-1 | 3042 | 881 | 0·706666 | 0·000016 | |
| | | PAR219P2b-2 | 3004 | 734 | 0·706735 | 0·000018 | |
| | | PAR219P2b-3 | 2674 | 690 | 0·706724 | 0·000024 | |
| | | PAR219P2b-4 | 2674 | 690 | 0·706788 | 0·000030 | |
| | Gm | PAR219Gm1 | 2022 | 854 | 0·706820 | 0·000024 | |
| | Gm | PAR219Gm2 | 2022 | 854 | 0·706816 | 0·000021 | |
| | Gm | PAR219Gm4 | 2022 | 854 | 0·706770 | 0·000022 | |
| PAR 011 | WR* | PAR11 | | 1714 | 0·706130 | 0·00004 | |
| | WR2005 | PAR11 | | 1714 | 0·706101 | 0·000011 | |
| PAR 068 | WR* | PAR68 | | 991 | 0·706920 | 0·00004 | |
| | WR2005 | PAR68 | | 991 | 0·706847 | 0·000015 | |
| | Low-Sr cores | PAR68P7-1 | 2208 | 643 | 0·706717 | 0·000015 | |
| | Rim | PAR68P7-2 | 2518 | 629 | 0·706810 | 0·000014 | |
| | High-Sr core | PAR68P9-1 | 3520 | 960 | 0·706688 | 0·000012 | |
| | High-Sr core | PAR68P9-1rpt | 3520 | 960 | 0·706680 | 0·000014 | |
| | Rim | PAR68P9-2 | 2547 | 689 | 0·706950 | 0·000021 | |
| | GmC | PAR068GmC | 2902 | 778 | 0·706886 | 0·000017 | |
| | GmC | PAR068GmCrpt | 2902 | 778 | 0·706893 | 0·000015 | |
| *Healing Flows* | | | | | | | |
| PAR 084 | WR2005 | PAR084 | | 1144 | 0·706610 | 0·000011 | |
| | Core | PAR084P3-6 | 3225 | 1123 | 0·706749 | 0·000027 | |
| | | PAR084P3-5 | 2809 | 922 | 0·706824 | 0·000017 | |
| | Intermediate | PAR084P3-4 | 2395 | 780 | 0·706853 | 0·000013 | |
| | | PAR084P3-3b | 2208 | 618 | 0·706803 | 0·000012 | |
| | | PAR084P3-3 | 2391 | 653 | 0·706832 | 0·000019 | |
| | | PAR084P3-2 | 2391 | 653 | 0·706742 | 0·000016 | |
| | Rim | PAR084P3-1 | 3180 | 892 | 0·706674 | 0·000013 | |
| | Gm | PAR084Gm1 | 2913 | 680 | 0·706608 | 0·000021 | |
| *Old Cone* | | | | | | | |
| PAR082 | WR* | PAR082 | | 1117 | 0·70670 | 0·00004 | |
| | WR2005 | PAR082 | | 1117 | 0·706678 | 0·000009 | |
| | Core | PAR082P4-2 | 2181 | 339 | 0·706812 | 0·000014 | |
| | Resorbed rim | PAR082P4-1 | 3478 | 1185 | 0·706744 | 0·000017 | |
| | Gm crystals | PAR082GmC | 3478 | 1214 | 0·706705 | 0·000010 | |
| | Groundmass | PAR082Gm | 3478 | 1214 | 0·706722 | 0·000023 | |
| | Pl in San | PAR082P0 | 1718 | 184 | 0·706785 | 0·000016 | |
| | Pl around San | PAR082P1 | 1798 | 209 | 0·706751 | 0·000013 | |
| | P5 (Osc) | PAR082P5 | 1703 | 186 | 0·706746 | 0·000014 | |
| | P13 (HSr core) | PAR082P13 | 3224 | 887 | 0·706667 | 0·000017 | |
| | Sanidine | PAR082S1 | 1400 | | 0·706869 | 0·000117 | |

(continued)

*Table 1: Continued*

| Sample | Zone type | Analysis name | Sr Plag | Sr liq | $^{87}Sr/^{86}Sr_c$ | 2SE | Comments |
|---|---|---|---|---|---|---|---|
| PAR165 | WR* | PAR165 | | 960 | 0·70668 | 0·00004 | |
| | WR2005 | PAR165 | | 960 | 0·706701 | 0·000008 | |
| | Core | PAR165P3-1 | 3102 | 1002 | 0·706586 | 0·000014 | |
| | Res | PAR165P3-2 | 2623 | 1036 | 0·706772 | 0·000016 | |
| | Rim | PAR165P3-3 | 2623 | 1036 | 0·706764 | 0·000011 | |
| | GM | PAR165Gm | 2722 | 866 | 0·706740 | 0·000019 | |
| PAR 130 | WR* | PAR130 | | 664 | 0·70702 | 0·00004 | |
| | WR2005 | PAR130 | | 664 | 0·706898 | 0·000008 | |
| Type IIb | Core | PAR130P18 | 3500 | 960 | 0·706484 | 0·000026 | |
| | Core | PAR130P28 | 3131 | 957 | 0·706554 | 0·000016 | |
| Type IIa | Core | PAR130P9core | 1699 | 337 | 0·706902 | 0·000016 | Glass contamination |
| | Core | PAR130P9core2 | 1699 | 337 | 0·706862 | 0·000015 | |
| | Core | PAR130P9core2rpt | 1699 | 337 | 0·706875 | 0·000032 | |
| Type I | Core | PAR130P1-8 | 2361 | 690 | 0·706719 | 0·000011 | |
| | | PAR130P1-8rpt | 2361 | 690 | 0·706727 | 0·000007 | |
| | | PAR130P1-7 | 749 | 750 | 0·706727 | 0·000010 | |
| | | PAR130P1-6 | 2445 | 759 | 0·706756 | 0·000009 | |
| | Zone after R1 | PAR130P1-5 | 2378 | 584 | 0·706731 | 0·000011 | |
| | | PAR130P1-4 | 2471 | 711 | 0·706680 | 0·000008 | |
| | | PAR130P1-3 | 2132 | 446 | 0·706746 | 0·000013 | |
| | | PAR130P1-3rpt | 2132 | 446 | 0·706738 | 0·000009 | |
| | | PAR130P1-2 | 2000 | 401 | 0·706819 | 0·000011 | |
| | Rim | PAR130P1-1 | 1762 | 361 | 0·706890 | 0·000015 | |
| | Rim | PAR130P1-1rpt | 1762 | 361 | 0·706907 | 0·000011 | |
| | Gm crystals | PAR130GmC | 1762 | 361 | 0·706986 | 0·000018 | |
| | Groundmass | PAR130Gm | 1762 | 361 | 0·706996 | 0·000025 | |

*Whole-rock data from Davidson *et al*. (1990), whereas WR2005 are the new whole-rock isotopic compositions.
$^{87}Sr/^{86}Sr_c$ are the values after correction for long-term drift between three periods of several weeks of analyses (drift between $2 \times 10^{-6}$ and $13 \times 10^{-6}$). Sr Plag (in ppm) are an average of microprobe analyses from Ginibre & Wörner (2007) over the drilled zone considered, and Sr liq concentrations (in ppm) are an average of Sr concentrations in the liquid calculated for each microprobe data point of the zone considered using the equation of Blundy & Wood (1991). Whole-rock Sr concentrations are indicated in the Sr liq column, even if the sample contains crystals. Pl, plagioclase; San, sanidine; Osc, oscillatory zoned, HSr, high Sr; Gm, groundmass; GmC, groundmass crystals; Res, resorbed zone; Rpt, repeat.

representative of the range in Sr concentrations (P0, Pl, P5, Pl3) in addition to the inner part and calcic rim of one typical crystal shown in Fig. 2a (P4).

Sr isotopic ratios of the Sr-poor plagioclase (P0, Pl, P4, P5) cores vary between 0·706812 ± 14 and 0·706744 ± 14 and are thus similar to those of the Rhyolite Dome whole-rock samples, which supports the hypothesis of mixing between such a rhyolitic component and a basaltic andesite. The lower isotopic ratio at 0·706667 ± 17 in the analysed Sr-rich plagioclase core (Pl3) suggests a complex mixing history in the rhyolitic component itself.

The rim grown after the resorbed zone in P4 has an isotopic ratio of 0·706744 ± 17, whereas groundmass and groundmass crystals (microlites) have ratios of 0·706722 ± 23 and 0·706705 ± 10 respectively, all only slightly lower than the Sr-poor inner part of P4, and slightly higher than the Sr-rich core (Pl3). The rims and groundmass crystals are significantly more radiogenic than would be expected from recharge with an unradiogenic high-Sr magma similar to the Upper Ajata lavas.

In PAR 165, all crystals show similar chemical zoning in major and minor elements. Therefore, we chose only one crystal (P3) and analysed the core, resorption zone and outer zone, as well as groundmass crystals. As expected, the higher-Sr core has less radiogenic Sr (0·706586 ± 14) than the resorption zone and rim, which are identical within error (0·706772 ± 16 and 0·706764 ± 11). These results are consistent with growth of the core from a fairly
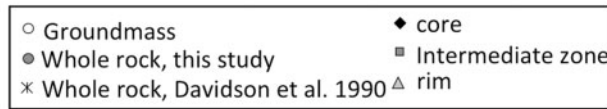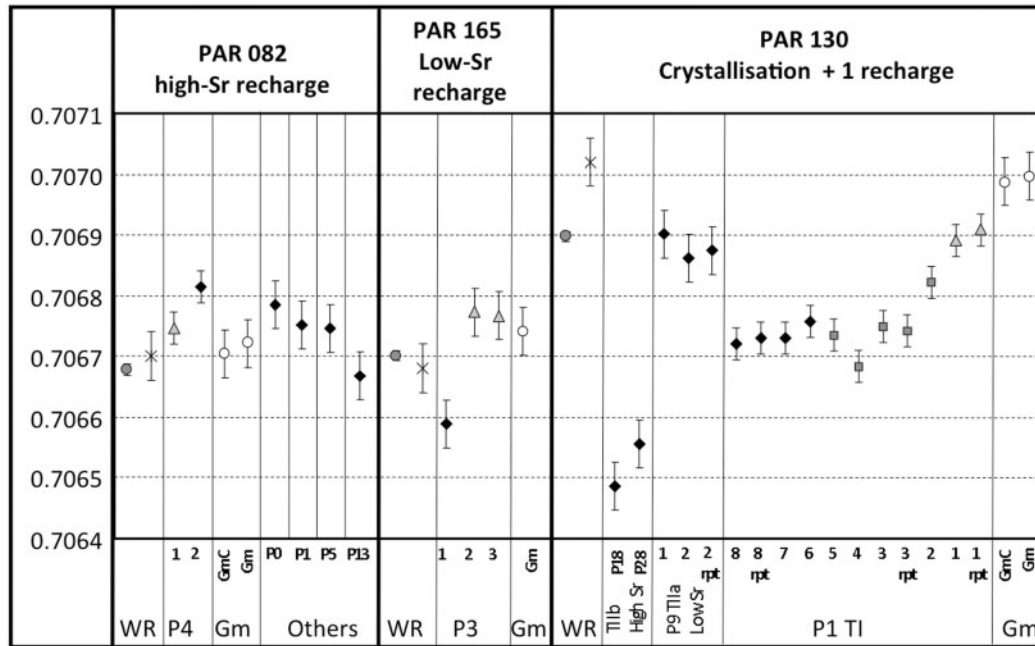
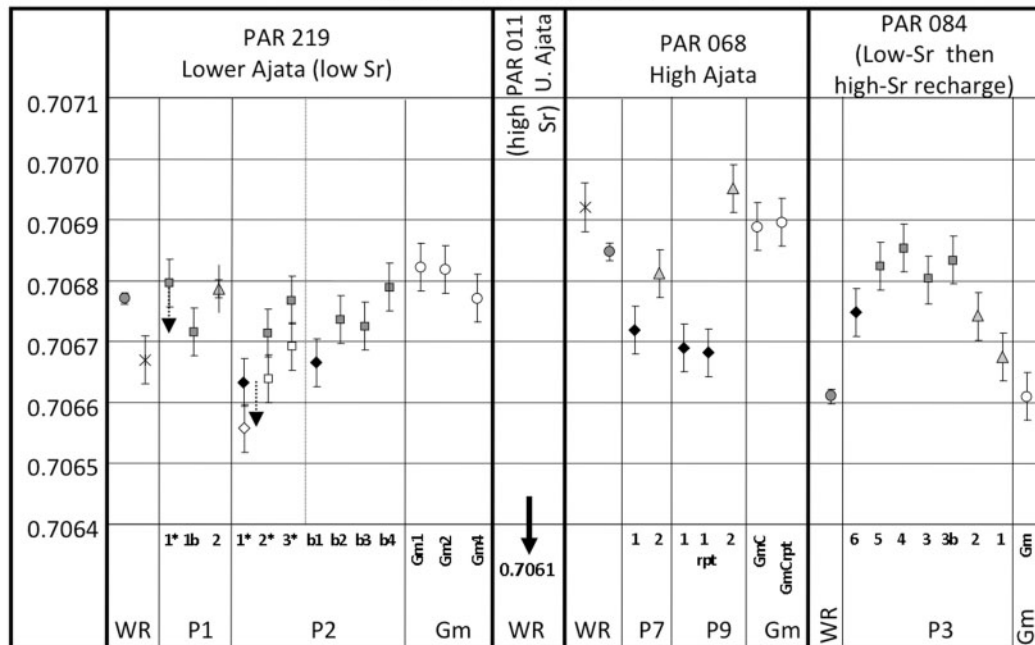**Fig. 5.** $^{87}$Sr/$^{86}$Sr data for all drilled samples and whole-rocks. Values are normalized to NBS987 = 0·710250. PAR 011 is aphyric and hence only the whole-rock value was analysed. Plagioclase crystals from a given sample are denoted P1–P*n*. Zone numbers are those shown in Figs 2–4 for representative crystals. Crystals not shown in Figs 2–4 were drilled only in the cores. In PAR 219, zones with a star were contaminated by the underlying glass during sampling of the thin section and the measured values are therefore too high; the arrow shows the estimated necessary correction. Error bars are set to 0·000040 to take into account the blank contribution, except for PAR 130 P1 and PAR 082 P4, where the error bar is set to 0·000025, given that the large drilled zones contain more than 10 ng Sr.
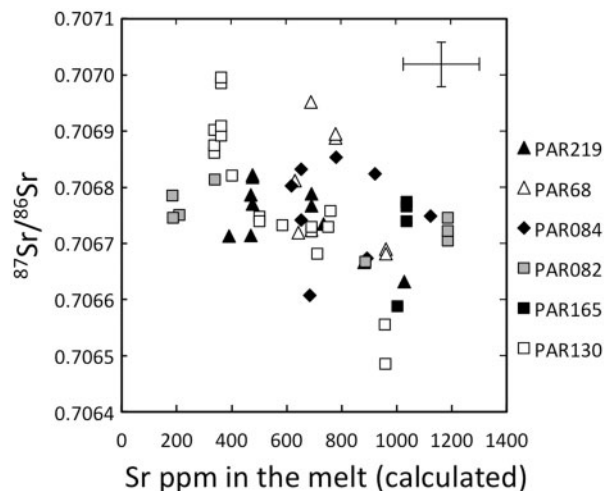
**Fig. 6.** Sr isotopic ratios of all microdrilled zones vs calculated Sr concentration in the liquid [calculated from the data of Ginibre & Wörner (2007)]. Average error bars are indicated. The reported uncertainty on Sr concentration in the melt (150 ppm) includes a term from the analytical uncertainty of the electron microprobe (50 ppm on the calculated Sr melt), the effect of 50°C uncertainty on the temperature (50 ppm) and the effect of an uncertainty on the coefficients in the equation (50 ppm). The reported error bar for Sr isotopic ratios takes the blank contribution into account.

evolved, relatively unradiogenic high-Sr magma and later mixing with a more mafic, more radiogenic, low-Sr magma, as indicated from the chemical zoning and comparison with the chemical and isotopic characteristics of the Ajata lavas. It should be noted, however, that the lowest isotopic ratio (core) is still significantly higher than that of Upper Ajata lavas.

In PAR 130, all three types of crystals [I, IIa and IIb of Ginibre *et al.* (2002)] as well as groundmass and groundmass crystals were analysed (Figs 2 and 5). In crystal Pl (Type I), eight zones were drilled (width 50–200 μm) parallel to the crystal faces, shown in Fig. 2c. Because of inaccuracy of the drilling path along different crystal faces, zones l and 2 were mixed with a small amount of the next one inward, which tends to smooth slightly the variations obtained. The intermediate value of zone 5 also represents the mixing of two chemically different zones during sampling, as could be seen after drilling. The actual change in isotopic ratio is therefore most probably more abrupt than observed. The smaller surface area of the core in the thin section makes it difficult to sample, and therefore the isotopic composition of the real core was not analysed. The observed isotopic profile in Pl mostly correlates negatively with the chemical variations (An, Fe and Sr profile). In the core the variations are small, outside the in-run analytical error but possibly within the uncertainty of blank contribution, and show a slight increase in $^{87}Sr/^{86}Sr$ ratio $(0.706719 \pm 11$ to $0.706756 \pm 9)$ rimward. A clear decrease to $0.706680 \pm 8$ occurs at the resorption surface Rl,

followed by a strong increase towards the rim, where the $^{87}Sr/^{86}Sr$ ratio reaches $0.706907 \pm 9$.

The An-rich patchy-zoned core of a Type IIa crystal (P9) gave a $^{87}Sr/^{86}Sr$ of $0.706872 \pm 15$. This zone was inferred from chemical zoning (An content, resorption surface morphology, Sr, Fe and Mg concentrations) to be equivalent to the R2 resorption zone of crystal Pl (between zone l and 2), where it is too small to be analysed. The value is higher than that of zone 2 and lower than that of zone l in Pl, inward and outward, respectively, of the resorption surface R2. Groundmass and groundmass crystals have higher $^{87}Sr/^{86}Sr$ than all zones of the large crystals. This is what is expected if the isotopic ratio is increasing rapidly towards the rim, and therefore averaged, over the 100 μm wide zone l of Pl, to a lower value than that of the outermost rim and the groundmass crystals. Sr-rich cores of Type IIb plagioclase (Pl8 and P28) show the lowest $^{87}Sr/^{86}Sr$ ratios found in Parinacota plagioclase $(0.706484 \pm 26$ and $0.706554 \pm 16)$.

The observed Sr isotopic systematics in PAR 130 adds further constraints to the published chemical zoning study of Ginibre & Wörner (2007). Whereas the chemical zoning can mostly be explained by closed-system evolution for Type I crystals, progressive contamination (open-system) is clearly evident from the $^{87}Sr/^{86}Sr$ values, which, as a consequence, increase towards the rim, reflecting the influence of a radiogenic component during crystal growth. This contamination is limited in the first part of the profile of the Type I crystal and much more significant in the part rimward of the resorption surface Rl. The recharge event suggested by Ginibre & Wörner (2007) is also confirmed by the lower $^{87}Sr/^{86}Sr$ ratio after the resorption surface Rl (Fig. 2c). In contrast, the R2 An peak does not seem to lower $^{87}Sr/^{86}Sr$ or change the slope of its increase. In fact, $^{87}Sr/^{86}Sr$ in the core of PAR 130 P9 (equivalent to R2) is intermediate between the values for zone l and 2, and suggests continued contamination associated with this resorption surface. The absence of an Fe and Mg increase after the dissolution surface indicates that no mafic recharge is involved here (Ginibre *et al.*, 2002) and that rather a change in temperature or water pressure is responsible for the dissolution. Based on an observed decrease in the Ba concentration of the melt towards the rim of the plagioclase, in the absence of crystallizing sanidine or biotite, Ginibre *et al.* (2002) suggested mixing with a more evolved melt closer to the magma chamber wall, with higher water concentration that causes resorption of plagioclase and a locally higher An content. The increased $^{87}Sr/^{86}Sr$ suggests involvement of the country rock, which is consistent with increasing interaction with the magma chamber margin. The detailed record of Sr evolution in the PAR 130 Pl crystal makes it an ideal case for AFC modelling including recharge, which we address in a later section.

The lower $^{87}Sr/^{86}Sr$ of the high-Sr cores is consistent with a parent magma related to the Upper Ajata. These ratios are, however, significantly higher than Upper Ajata whole-rock data, suggesting that, if the parent magma was similar to the Upper Ajata magma, some additional contamination occurred before plagioclase crystallization.

### Healing Flows

In PAR 084, we drilled only one crystal, as the zones with very different chemistry are narrow and it was difficult to avoid mixing in the outermost few zones. However, a general pattern of $^{87}Sr/^{86}Sr$ negatively correlated with Sr content is observed: the high-Sr core and rim both have the lowest isotopic ratio, and the low-Sr middle zone the highest isotopic ratio. This is consistent with the influence of a high-Sr unradiogenic magma (Upper Ajata type) in the core and in the rims (more mafic in the rim as seen from the higher Fe content), and an intermediate zone influenced by recharge of a low-Sr, more radiogenic mafic magma (Lower Ajata type), as suggested by Ginibre & Wörner (2007). Crustal contamination therefore is not evident here.

## Ajata Flows

In PAR 219, Lower Ajata magmas contain rare but generally large plagioclase crystals, interpreted from the chemical zoning patterns as antecrysts (Ginibre & Wörner, 2007), which may influence the bulk Sr isotopic composition of the magma. We therefore analysed the plagioclase crystals (P1, not shown, and P2, Fig. 4a) and the groundmass to quantify disequilibrium between crystal and melt and to determine the isotopic composition of the low-Sr mafic magma. Zones P1-1 and P2-1, -2 and -3 were sampled too deeply, resulting in some limited contamination by the underlying glass $(^{87}Sr/^{86}Sr = 0.721404 \pm 14)$ and a measured value that was, therefore, too high. We thus reanalysed similar zones in the same crystals (denoted P1-1 b, P1-2, and P2b-1, -2, -3, -4). However, the contaminated zone P2-1 is the high-Sr core with the lowest $^{87}Sr/^{86}Sr$ ratio, and the zone was too small to be sampled again. Therefore, we include the data and estimate the necessary correction by comparison between uncontaminated and glass-contaminated zones (P1-1 and -1 b). The contaminated value is about 0.00008 too high. As a result, the lowest $^{87}Sr/^{86}Sr$ found in PAR 219 is estimated at $0.70655 \pm 2$. Rims of crystal P1 and the other more resorbed crystal (P2) have higher isotopic ratios $(0.7066714 \pm 17$ to $0.706798 \pm 15)$. Three groundmass analyses (different drilled samples) agree within error $(0.70680 \pm 2)$. Textural and chemical evidence (highly calcic, Fe- and Mg-rich rims, diversity of internal zoning patterns) indicates that the plagioclase crystals are antecrysts. However, the Sr concentration and $^{87}Sr/^{86}Sr$ of most zones are fairly close to the groundmass value, except for the high-Sr cores, suggesting that they are not completely unrelated to the PAR 219 groundmass magma. Because of the disequilibrium between plagioclase and groundmass, the low-Sr mixing end-member considered for other Parinacota samples should be the groundmass of PAR 219, rather than bulk PAR 219. The Sr concentration of the groundmass, calculated from the plagioclase rims and microlites using partitions coefficients, as described above, is 854 ppm. The same concentration calculated by subtracting the Sr contained in 2% plagioclase with 2800 ppm Sr from the whole-rock concentration is 765 ppm, within error of the value calculated using partition coefficients. The $^{87}Sr/^{86}Sr$ of the groundmass $(0.70680 \pm 2)$ is significantly higher than the old whole-rock value $(0.70667 \pm 4)$, but only slightly higher than the new whole-rock value $(0.706771 \pm 8)$.

In PAR 068 (High Ajata), we drilled only two crystals, one with a high-Sr core (P9, not shown), the other one with a lower-Sr core (P7, Fig. 4b). Because of the diversity of the size of crystal cores, this is probably not completely representative. Some cross-contamination between zones was observed during drilling owing to breakage of the remaining zone. Cross-contamination was exacerbated by the crystals being of relatively small size, and resorbed. P9 core (high-Sr) is slightly mixed with the resorbed zone (the true value is probably lower). The isotopic difference between the high-Sr (P9) and low-Sr (P7) cores is relatively small and within blank uncertainty $(0.706682 \pm 14$ and $0.706719 \pm 15$, respectively), and therefore in this case not correlated with Sr concentration. This could be partly caused by mixing of the Sr-rich core with the external zone during drilling. The isotopic ratio of the rim of P9 is close, albeit slightly higher than those of the groundmass crystals and within error of blank contamination, given the small size of the drilled zones. This blank contribution probably explains the observed difference (we are confident that the P9 rim sample has not been contaminated by underlying glass) although real small-scale heterogeneity cannot be completely ruled out. The rim of P7 has an isotopic ratio of $0.706812 \pm 14$, lower than those of P9 rim and the groundmass crystals, even when taking into account a blank contribution of 0.00004. This rim was drilled after the core, and part of the remaining core broke, resulting in a mixed analysis for the rim, which should explain the discrepancy. We therefore consider the value of the groundmass crystals as a minimum for the melt just before eruption. In any case, this value is more radiogenic than the low-Sr, high $^{87}Sr/^{86}Sr$, Lower Ajata type mafic end-member and reflects additional contamination.

## Summary of crystal isotope data

The isotopic data partly confirm the results of Ginibre & Wörner (2007), who showed that the chemical zoning of Parinacota plagioclase can be explained mainly by mixing between two mafic and one evolved end-members, with possibly some additional fractionation. The inferred

Sr concentration of the melt in equilibrium with the new crystal growth zone (after recharge) is qualitatively negatively correlated with its $^{87}Sr/^{86}Sr$ (Fig. 6). This is consistent with recharge with alternating mafic end-members, one with high Sr and low $^{87}Sr/^{86}Sr$, the other with low Sr and high $^{87}Sr/^{86}Sr$. However, two samples, one evolved (dacite PAR 130) and one more mafic (mafic andesite PAR 068), show a range of $^{87}Sr/^{86}Sr$ recorded in plagioclase that significantly exceeds the upper end of the range found in the assumed Ajata type end-members and therefore must have involved some additional crustal contamination. For some other samples, the effect of contamination is less clear, but mixing between the three end-members is not sufficient to explain quantitatively the variations of Sr concentrations and isotopic ratios (e.g. PAR 082). It is noteworthy that no plagioclase crystals record the very low $^{87}Sr/^{86}Sr$ of the aphyric magma PAR 011 ($0.706114 \pm 11$), the lowest value being $0.706484 \pm 26$. This observation suggests that plagioclase crystallization occurred after some initial contamination, at least enough to increase the magma $^{87}Sr/^{86}Sr$ to 0.706486.

# EC-AFC MODEL OF PAR 130-P1

The detailed record of Sr isotope evolution in crystal PAR 130-P1 reflects crustal assimilation during crystallization of plagioclase and provides a detailed time series of magma evolution that lends itself to quantitative modelling. Such assimilation processes in the upper crust can be modelled by solving a set of equations involving the chemical and isotopic compositions of the magmas, crust, crystallizing minerals and partition coefficients and other parameters depending on the model used [assimilation, fractional crystallization (AFC): De Paolo, 1981; recharge, assimilation, fractionation, tapping (RAFT): Aitcheson & Forrest, 1994; energy-constrained AFC (EC-AFC): Spera & Bohrson, 2001, 2004].

Below we present what we believe is the first attempt to quantify fully the evolution of a magma from the core–rim profile of a single feldspar crystal. Such quantification represents a further advance in the value of single crystals in revealing magma evolution [see, for example, the single crystal feldspar and zircon studies of Morgan *et al.* (2007) and Klemetti *et al.* (2011), respectively]. As such we consider each of the parameters of the model in some detail below, paying particular attention to the degree to which they can realistically be constrained and the degree to which the model is sensitive to them. At the outset we must recognize that 'the magma' is not a simple self-contained entity. Open-system processes such as contamination and mixing are clearly occurring, as described above. These processes can be recognized and quantified only from the 'reference frame' of the crystal as it moves through, and grows in, the magma system. Like a stratigraphic record of the paleoenvironment, the crystal growth zones record variations in the growth environment, along with gaps in the record through time (resorption surfaces in the case of the crystal or unconformities in a sequence of sedimentary rocks) when no deposition is occurring.

## Model details

We use the EC-E'RAχFC model of Spera & Bohrson (2004) including assimilation and recharge, but not using the eruption function, although eruption of part of the magma reservoir before eruption of the PAR 130 magma cannot be ruled out. Input parameters of the model are explained in Table 2. The model involves three components of the magmatic system: the resident magma, the country rock and the recharge magma. For each of these components, various parameters are set as input data, including liquidus, solidus and initial temperature, melt fraction evolution with temperature (a and b parameters determining the shape of the melt fraction curve), chemical and isotopic composition, partition coefficients, amount of recharge magma and recharge temperature. The thermal coupling between wall-rock and magma is set using the parameter Teq (equilibration temperature): this temperature is not directly a physical temperature in the system but is chosen arbitrarily in the model and is related to the amount of country rock interacting thermally with the magma: Teq is high if the heated portion of the country rock is small.

The output parameters of the model are the evolution of the amount and compositions of the different phases (melt, solid) as a function of decreasing temperature, which can be compared with a known evolution. Such models are usually used with a large number of trace elements and isotopes to match the evolution of a rock series including numerous samples. Here, the evolution to be modelled is that of the melt in one sample (PAR 130) during plagioclase crystallization, as recorded in the different zones of the crystal. We use only Sr concentration and Sr isotopic ratio. The Sr concentration in the melt at the time of growth of a zone is calculated, via the appropriate $Kd_{Sr}$, from the concentration measured in the crystal in that zone and the isotopic ratio is taken directly from the microsampling data. As the modelled evolution is a function of temperature, we also need to estimate the temperature at which each of the zones grew, which then determines the melt fraction curve and the temperature chosen for recharge. The calculation results then provide (1) Sr isotope evolution, which can be matched to the observed $^{87}Sr/^{86}Sr$ variations, (2) values of arbitrarily set parameters such as Teq necessary to match the data and (3) output parameters such as the melt fraction in the country rock and the percentage of assimilated crust at a given temperature or Sr isotopic ratio.

The model EC-E'RAχFC has the advantage that it takes thermal constraints into account but has three main limitations where it does not reflect reality well, mainly owing

*Table 2: EC-RAFC parameters for PAR 130 reference case, without recharge and with recharge (scenario 1)*

| Parameter | Description | No recharge | With recharge | Unit |
|---|---|---|---|---|
| Tlm = Tm0 | Liquidus temperature of the resident magma = initial temperature of the magma | 1050 | 1050 | °C |
| Tla | Liquidus temperature of the crust | 900 | 900 | °C |
| Ta0 | Initial temperature of the crust | 300 | 300 | °C |
| Tlr = Tr0 | Liquidus temperature of the recharge magma = initial temperature of the magma | | 1100 | °C |
| Ts | Solidus temperature of all components | 750 | 750 | °C |
| cpm | Isobaric specific heat capacity (resident magma) | 1450 | 1450 | J kg$^{-1}$ K$^{-1}$ |
| cpa | Isobaric specific heat capacity (crust) | 1370 | 1370 | J kg$^{-1}$ K$^{-1}$ |
| cpr | Isobaric specific heat capacity (recharge magma) | | 1450 | J kg$^{-1}$ K$^{-1}$ |
| hm | Latent heat of fusion/crystallization (resident magma) | 310000 | 310000 | J kg$^{-1}$ |
| ha | Latent heat of fusion/crystallization (crust) | 270000 | 270000 | J kg$^{-1}$ |
| hr | Latent heat of fusion/crystallization (recharge magma) | | 310000 | J kg$^{-1}$ |
| magma a | Melting curve parameter (resident magma) | 250 | 250 | |
| magma b | Melting curve parameter (resident magma) | 13 | 13 | |
| assim a | Melting curve parameter (crust) | 250 | 250 | |
| assim b | Melting curve parameter (crust) | 13 | 13 | |
| recharge a | Melting curve parameter (recharge magma) | | 250 | |
| recharge b | Melting curve parameter (recharge magma) | | 13 | |
| Tri | Temperature at which magma recharge occurs | 940 | | °C |
| Mr0 | Mass of recharge magma normalized | | | |
| | to the mass of initial resident magma | | 0·28 | |
| Srm | Initial Sr concentration of the resident magma | 750 | 750 | ppm |
| D0m | Temperature-dependent Sr partition coefficients (magma): | 0·0017189 | 0·0017189 | |
| ΔHm | $D_{Sr}m(T) = D_0m.exp(-\Delta Hm/RT)$ ($T$ in Kelvin) | 77690·976 | 77690·976 | J kg$^{-1}$ |
| Sra | Sr concentration of the assimilated crust | 382 | 382 | ppm |
| D0a | Temperature-dependent Sr partition coefficient (crust): | 0·0755636 | 0·0755636 | |
| ΔHa | $D_{Sr}a(T) = D_0a.exp(-\Delta Ha/RT)$ ($T$ in Kelvin) | 36863·409 | 36863·409 | J kg$^{-1}$ |
| Sr r | Sr concentration of the recharge magma | | 1000 | ppm |
| D0r | Temperature-dependent Sr partition coefficient (recharge): | 0·0017189 | | |
| ΔHr | $D_{Sr}r(T) = D_0r.exp(-\Delta Hr/RT)$ ($T$ in Kelvin) | | 77690·976 | J kg$^{-1}$ |
| 87/86m | Initial Sr isotopic ratio of resident magma | 0·70675 | 0·70675 | |
| 87/86a | Sr isotopic ratio of assimilated crust | 0·71278 | 0·71278 | |
| 87/86r | Initial Sr isotopic ratio of recharge magma | | 0·70648 | |
| Teq | Equilibration temperature | 913 | 895 | °C |

to the fact that the model assumes thermal equilibrium rather than heat transfer.

(1) The evolution is calculated with decreasing temperature, therefore no temperature increase after recharge occurs in the model. The heat of the recharge magma is used for enhanced assimilation of the wall-rock and the change in crystal chemistry (An and Sr) is driven by only the composition of the new magma. In reality, a recharge event with a hot magma will cause an increase in temperature of the system and dissolution of the crystals, as seen in the crystal by a resorption surface (R1). The observed subsequent increase in An and Sr content is thus partly caused by the melting of plagioclase, which is not taken into account in the model. More importantly, the equivalence that we use between spatial profile and decreasing temperature does not accurately reflect the reality, where temperature is not monotonously decreasing.

(2) The equilibration temperature is set arbitrarily for the whole evolution, including the recharge event, and the modelled evolution before recharge is thus not independent of the later recharge as it should be. For this reason, we first use the model without recharge

to fit the behaviour of the system before recharge and then the model with recharge for the behaviour after recharge.

(3) The melting curves of the resident magma, recharge magma and country rock are set for the whole calculation. The possibility of a wetter recharge magma that would bring water into the system and consequently modify the curves for country rock and resident magma cannot be taken into account. In the same way, the release of water by the assimilated crust that could add water to the resident magma and modify its melt fraction curve cannot be taken into account directly.

For all these reasons, we do not attempt to reproduce accurately the details of the observed $^{87}Sr/^{86}Sr$ evolution with time (core–rim), especially around the resorption surface. However, by varying parameters such as the initial temperature of the resident magma, the crust and recharge magma, initial compositions and equilibrium temperature in the model we obtain useful constraints on the conditions of emplacement and recharge, and on the amount of crustal assimilation.

## Parameters and petrological–geochemical constraints for sample PAR 130-P1

In the model, the starting magma (dacite) is emplaced into the crust at its liquidus temperature and starts assimilating the upper crust after emplacement, while cooling and crystallizing. The magma reservoir is then replenished by the recharge magma, cooling again and crystallizing until erupting to produce sample PAR 130.

Some parameters are determined with petrological or geochemical constraints. Others are not well constrained but we vary them to see their effects on modelling results as specified below. Table 2 shows all the parameters for one reference case, both without recharge and with a mafic recharge as described in scenario 1 in the recharge hypotheses section. Non-linear logistical melt fraction functions used for the various components are shown in Fig. 7a. All parameters used for the modelling can be found in the Electronic Appendices 1 and 2 respectively (supplementary material is available for downloading at http://www.petrology.oxfordjournals.org).

### Constraints on temperature

Fe–Ti oxide thermometry based on microprobe analyses (Electronic Appendix 3), and the model of Stormer (1983), are used to constrain the temperature through time profile (Fig. 8). The eruption temperature is estimated from oxide pairs where both phases are in contact. The oxides are zoned between their cores and the ilmenite–magnetite contact. Analysed points were taken in equivalent zones of each phase from a given pair and are in equilibrium following the test of Bacon & Hirschmann (1988). The lowest

temperature (830–850°C) is found at the phase contact and probably corresponds to re-equilibration during ascent or after eruption in the dacite dome. The highest temperatures are found in the cores (908°C) and are more likely to represent minimum pre-eruptive temperatures. Therefore we chose 910°C as the eruption temperature for the model. Such a high temperature for a dacite suggests a low water content, which is consistent with the abundant pyroxene and low biotite and amphibole content of the sample. This is also consistent with the conclusion from trace element zoning (Ginibre *et al.*, 2002) suggesting an increase in water content after resorption R2, which necessitates a water-undersaturated magma.

The recharge temperature is more difficult to estimate. Some oxide pairs, in particular one included in the external zone of an orthopyroxene crystal, albeit non-touching, indicate a temperature between 935 and 940°C using the same thermometer. The slower diffusion through orthopyroxene reduces equilibration after entrapment, but the presence of this oxide pair in the same zone suggests that the oxides were in equilibrium during the growth of this zone (Fig. 8). This may therefore represent the temperature shortly after recharge, and thus we use 940°C as the temperature at which recharge occurs. Owing to the unreliability of this temperature estimate [it fails the Bacon & Hirschmann (1988) test because the oxides are not in contact] we consider it indicative at best, and have therefore tested the effect of varying the recharge temperature (from 930 to 970°C).

Because reheating and dissolution of the crystal are not taken into account in the model, it is not strictly possible to match a decreasing temperature scale with the profile in the crystal. Moreover, the drilled zone preceding the recharge horizon was mechanically mixed with the subsequent zone during sampling so the exact $^{87}Sr/^{86}Sr$ ratio just before recharge is not known. Figure 8 shows our interpretation of the temperature profile. For simplicity, it is considered linear with distance in the crystal, which is probably not the case, even outside the zone where the recharge occurs. We discuss this issue in the interpretation section below.

For the resident magma, we tested two liquidus temperatures (1000 and 1050°C; Fig. 7a) and adjusted the melt fraction curve to match the estimated crystal fraction in the sample: less than 10% at the recharge temperature, 20% upon eruption.

### Constraints on assimilant composition

Clearly, we cannot confidently constrain the composition of the assimilated crust from the ~70 km section beneath Parinacota; we therefore compare the effect of several potential contaminant compositions. Metamorphic basement in the region is exposed in the Belén region (within 100 km of Parinacota) and includes a variety of lithologies (Aitcheson *et al.*, 1995) ranging from silicic gneiss to more mafic compositions (metadiorite and augengneiss)
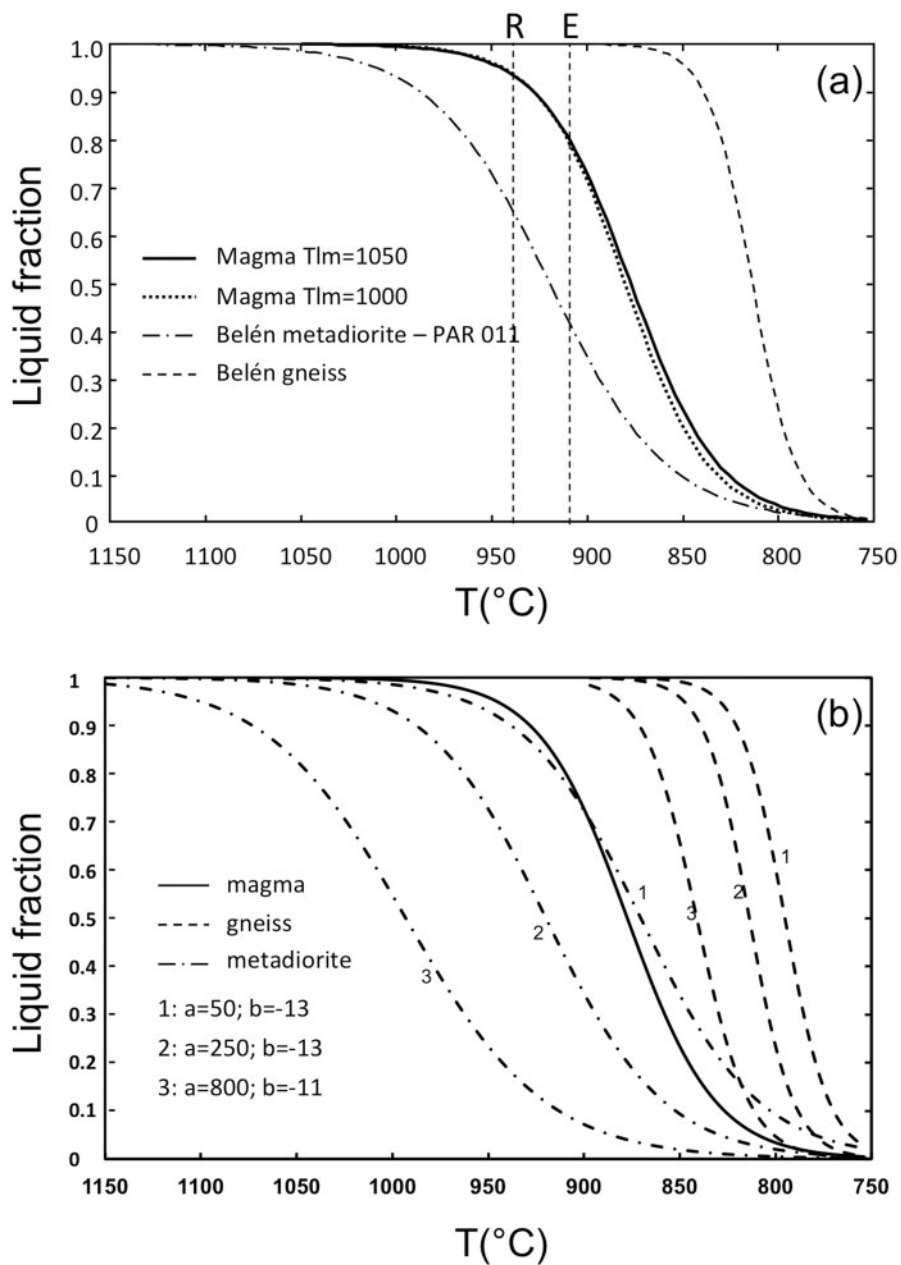
**Fig. 7.** (a) Liquid fraction curves for the various components used in the EC-RAFC model with parameters a and b set to (250, −13). Dashed vertical lines at 940 and 910°C represent recharge (R) and eruption (E) temperatures and intersect the liquid fraction curve of the magma at ∼6% and 20% crystals respectively. Belén metadiorite and PAR 011 are shown by the same curve because of their similar major element compositions. (b) Variations of the liquid fraction curves with various values of the parameters a and b.

(Table 3). Other potential contaminant lithologies, albeit with a more limited isotopic contrast, include older magmatic rocks (ignimbrites or their plutonic roots).

Variations in assimilated lithologies will have two types of effect. First, the amount of anatectic melt depends on the melt fraction curve of the country rock and thus mainly on major elements: we take the Belén gneiss composition as an example of fertile crust with an assumed liquidus temperature of 900°C and the augengneiss and

metadiorite as refractory crust, with assumed liquidus temperature of 1150°C. Variations in the a and b parameters of the non-linear logistical melt fraction function for the gneiss and the metadiorite (Fig. 7b) allow us to test the effect of the fertility of the crust more in detail.

Second, we test the influence of the variations in Sr content and Sr isotope composition of the country rock on the melt evolution by using a melt fraction curve similar to the gneiss, a Sr concentration of 300 ppm and $^{87}Sr/^{86}Sr$
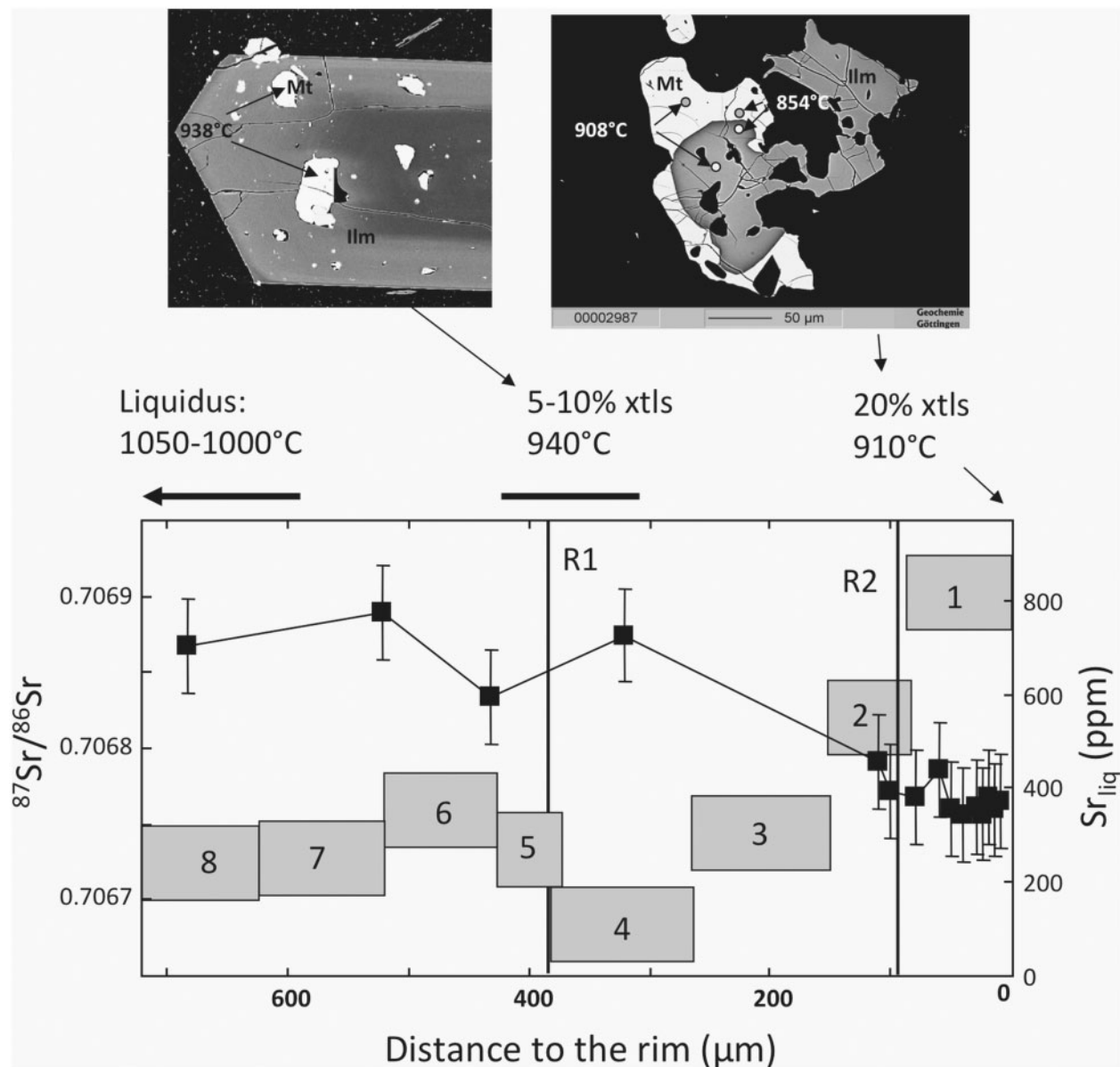
**Fig. 8.** Data and petrological constraints used for the EC-RAFC model of PAR 130. Core–rim profile represents evolution through time of magma from which crystal PAR 130 grew (see Fig. 2c). Grey boxes 1–8 are $^{87}Sr/^{86}Sr$ values (incorporating in-run error and blank contribution); black squares are Sr contents in the melt (Table 1). Eruption temperatures are determined from oxide–oxide pairs as indicated in the photomicrographs above (see text). R1, R2 represent recharge events, marked by resorption surfaces (see Fig. 2c); xtls, crystals. The eruption temperature 910°C is assumed to correspond to the rim of the crystal (zone 1). The horizontal bar below 940°C shows the interval in the profile that may correspond to this temperature in the model, because reheating following recharge is not accounted for by the model.

of 0·708 as representative of a felsic magmatic country rock. We also test both the augengneiss and metadiorite as mafic lithologies as they have slightly different Sr contents and isotope ratios.

### Constraints on recharge magma composition

Petrological constraints on the recharge magma can be gained from the high-Sr cores in PAR 130 plagioclase. These are rare and each of the three crystals analysed by

Ginibre *et al.* (2002) showed a sharp boundary that may be simultaneous with the R1 recharge in Type I crystals (from the variable size of subsequent zones) and a resorption discontinuity that can be compared with R2. It is therefore most likely that these high-Sr cores were introduced with the recharge magma. They can either be in equilibrium with the liquid or they may be antecrysts from the recharge magma, collected during ascent to the resident magma. In the first case, their Sr concentration

*Table 3: Composition of Belen basement rocks*

| Rock type | Gneiss | Metadiorite | Augengneiss |
|---|---|---|---|
| $SiO_2$ | 68·27 | 54·49 | 52·59 |
| $TiO_2$ | 0·40 | 0·99 | 1·06 |
| $Al_2O_3$ | 15·36 | 16·46 | 17·31 |
| $Fe_2O_3$ | 2·00 | 4·10 | 3·55 |
| FeO | 2·21 | 5·80 | 6·64 |
| MnO | 0·11 | 0·20 | 0·20 |
| MgO | 1·53 | 4·42 | 4·91 |
| CaO | 4·93 | 7·06 | 6·88 |
| $Na_2O$ | 3·10 | 2·65 | 2·54 |
| $K_2O$ | 0·84 | 1·55 | 1·57 |
| $P_2O_5$ | 0·08 | 0·15 | 0·15 |
| LOI | 1·87 | 1·49 | 2·77 |
| Sum | 98·83 | 97·87 | 97·40 |
| Sr | 382 | 295 | 345 |
| $^{87}Sr/^{86}Sr$ | 0·71278 | 0·71341 | 0·71189 |
| Assumed Tl | 900 | 1150 | 1150 |

Chemical and isotopic compositions are from Aitcheson *et al.* (1995). Assumed Tl are the liquidus temperatures used for the EC-RAFC model.

and isotopic ratio reflect the characteristics of the recharge magma; in the second case, other compositions for the recharge magma are possible. Therefore we consider three recharge scenarios: one with an andesite in equilibrium with high-Sr cores, one with a basaltic andesite similar to PAR 11, and one with a new batch of the initial dacite. For the first two scenarios, we assume that little or no contamination occurs in the dacite before the crystallization of the Pl core and choose an initial isotopic ratio close to those measured in the internal zones (0·70672). In the third one, the initial melt must have lower $^{87}Sr/^{86}Sr$ to allow the observed decrease in isotopic ratio after recharge.

*Scenario 1.* The recharge magma, in equilibrium with the high-Sr cores, has 1000 ppm Sr, calculated using the Blundy & Wood (1991) equation, and $^{87}Sr/^{86}Sr$ of 0·70648 (the lowest observed in Parinacota crystals). Mass balance shows that, to change the liquid composition from 600 ppm Sr at 0·70676 to 0·70665 by recharge, the relative mass Mr0 (mass of recharge magma normalized to original magma mass) necessary is 0·28. We use a melt fraction curve that is slightly more refractory than the original dacite. This scenario is considered the most plausible and therefore sensitivity studies are carried out using this set of parameters as a reference. We test two temperatures of the recharge magma (1050–1100°C).

*Scenario 2.* The recharge magma is a basaltic andesite similar to Upper Ajata PAR 011 (1760 ppm at 0·706114).

The Mr0 needed, calculated as above, is 0·065. The Sr content in the mixed magma for scenarios 1 and 2 is 676 and 729 ppm respectively, which is within error of the melt in equilibrium with the growth zone after recharge. We test two temperatures of the recharge magma (1150–1200°C).

*Scenario 3.* The recharge magma is similar to the uncontaminated initial dacite magma, at the liquidus temperature. We choose 0·70665 as initial isotopic ratio for both resident magma and recharge, and 750 ppm as initial Sr concentration (but the model is insensitive to initial Sr content). Mr0 is 2·09.

### Constraints on partition coefficients

Variations in Sr concentration in the melt extracted (owing to partial melting of the country rock) and in the crystallizing magma (owing to fractional crystallization) are taken into account in the model using bulk partition coefficients for all components. These bulk partition coefficients for Sr were estimated from the modal composition of the sample and plagioclase An content using the equation of Blundy & Wood (1991). Because the latter varies significantly with crystallization, variable bulk Sr partition coefficients are used in the model in the form of $D_{Sr} = D_0(\exp -\Delta H/RT)$. $D_0$ and $\Delta H$ were determined for each component using bulk $D_{Sr}$ estimated at liquidus and solidus temperature for country rock and recharge magmas, and at liquidus and eruption temperature from the core and rim composition of plagioclase phenocrysts for the dacite. Mineral assemblages at liquidus and solidus and/or eruption temperature, as well as the $D_0$ and $\Delta H$ inferred, are given in Electronic Appendix 4, for the initial dacite, two recharge magmas and two country rocks. For the latter, the An content of plagioclase is not well known, but the effect of 20% An variations in plagioclase on the modelled curve is less than 2°C for a given Sr content or $^{87}Sr/^{86}Sr$.

### Results (1); EC-E'RAFC modelling of PAR 130 P1 after emplacement and before recharge

We first consider the evolution before recharge (i.e. for temperatures above 940°C), by setting the mass of the recharge magma (Mr0) to zero. The variations in analysed isotopic ratios in this part of the crystals are small (possibly within error caused by blank contribution), but this modelling shows how sensitive the model is to various parameters and also whether the chosen scenarios are realistic. For each hypothesis, the parameters for all three components (magma, country rock and recharge magma) are set first and then several runs with various values of Teq are computed and the modelled Sr concentration and isotopic ratios are compared with the data. Other output data of the model include, as a function of temperature, the melt fraction in the country rock (fa) and the percentage of anatectic melt in the magma (Table 4). A set of parameters that fits the data well (crust = gneiss, Tlm = 1050,

*Table 4: Results of selected EC-AFC calculations*

| | Before recharge (Mr0 = 0) | | | | | With recharge | | | |
| | | | | | | Scenario 1 | | Scenario 2 | |
| | Ref. | Tlm = 1000 | assim = md | assim = ag | Ta0 = 600 | Tr0 = 1050 | Tr0 = 1100 | Tr0 = 1150 | Tr0 = 1200 |
|---|---|---|---|---|---|---|---|---|---|
| *Input parameters* | | | | | | | | | |
| $Tlm = tm0$ | 1050 | 1000 | 1050 | 1050 | 1050 | 1050 | 1050 | 1050 | 1050 |
| $Tla$ | 900 | 900 | 1150 | 1150 | 900 | 900 | 900 | 900 | 900 |
| $Tlr = Tr0$ | | | | | | 1050 | 1100 | 1150 | 1200 |
| $Ta0$ | 300 | 300 | 300 | 300 | 600 | 300 | 300 | 300 | 300 |
| $Tri$ | | | | | | 940 | 940 | 940 | 940 |
| $Sra$ | 382 | 382 | 295 | 345 | 382 | 382 | 382 | 382 | 382 |
| $^{87}Sr/^{86}Sr\ a$ | 0·71278 | 0·71278 | 0·71341 | 0·71189 | 0·71278 | 0·71278 | 0·71278 | 0·71278 | 0·71278 |
| $Sr\ r$ | | | | | | 1000 | 1000 | 1760 | 1760 |
| $^{87}Sr/^{86}Sr\ r$ | | | | | | 0·70648 | 0·70648 | 0·70611 | 0·70611 |
| *Output parameters* | | | | | | | | | |
| $Teq_{model}$ | 913·71 | 928·7 | 928·27 | 928·27 | 880·64 | 900 | 895 | 895 | 895 |
| $Ma0_{model}$ | 0·23 | 0·12 | 0·19 | 0·19 | 0·6 | 0·33 | 0·32 | 0·34 | 0·35 |
| $fa$ | 0·226 | 0·384 | 0·221 | 0·234 | 0·093 | 0·728 | 0·555 | 0·565 | 0·590 |
| %assim | 5·2 | 4·5 | 4·2 | 4·4 | 5·4 | 20·3 | 19·6 | 19·9 | 19·4 |

fa (melt fraction in the country rock) and the percentage of assimilated crust is for 0·70676 at 940°C (without recharge) or for 0·70700 at 905°C < $T$ < 910°C (with recharge for scenarios 1 and 2). Assim = md and assim = ag indicate the nature of the assimilated crust: metadiorite and augengneiss respectively, instead of gneiss when not stated.

Teq = 913°C) is taken as a reference as we vary different parameters to investigate their effect. The effects of the various parameters on the evolution of isotopic ratios with temperature are significant and are discussed below (Fig. 9a–d) whereas the effects on the evolution of Sr concentrations are small and are therefore not discriminant (Fig. 9e).

*Teq adjustment*

In some cases (eg. Ti = 1000, assimilant = metadiorite, Ta0 = 200°C; not shown), the desired isotopic ratio is just reached at Teq = $T_R$ (recharge temperature at 940°C), or, in the full model including recharge, the final isotopic ratio is not reached at Teq = $T_E$ (eruption temperature), ruling them out as potential model solutions. However, in most cases the model can match the data using an appropriate Teq. Therefore the effect and significance of Teq must be examined first and Teq necessary to fit the data both for Sr concentrations and Sr isotopic ratio, $Teq_{model}$, is one of the results of the modelling (Table 4).

Variations of 10°C in Teq, all other parameters being constant, causes about 10°C variations in the temperature at which a given $^{87}Sr/^{86}Sr$ is reached (Fig. 9a). In most cases, sufficient increase of isotopic ratio can be reached only with high Teq, in the magmatic temperature range.

At Teq, the system is supposed to be in thermal equilibrium (magma and a mass Ma0 of country rock are at Teq, and are thermally isolated from the surrounding rocks). Teq is the temperature at which the system stops evolving. This obviously does not occur in reality, because the mass of country rock interacting thermally with the magma will increase with time until the magma body reaches the temperature defined by the geotherm (Ta0). Therefore it could be expected that the model departs more from reality close to Teq than far above, and thus solutions in which the modelled evolution including the eruption temperature is close to Teq should be considered with caution, because the equilibrium model may differ from a more realistic time evolution.

The significance of Teq is better understood by considering Ma0: the mass of country rock interacting thermally with the magma depends on Teq [see Spera & Bohrson (2001) for a detailed discussion]. This mass may be compared with the size of the metamorphic aureoles around intrusions. A high Teq corresponds to a small Ma0: this may indicate that heat transfer is slow in the country rock, involving only conduction and no hydrothermal system. Alternatively or additionally, it may be related to the size or shape of the magma chamber: for a given rate of heat transfer Ma0 depends on the surface to volume
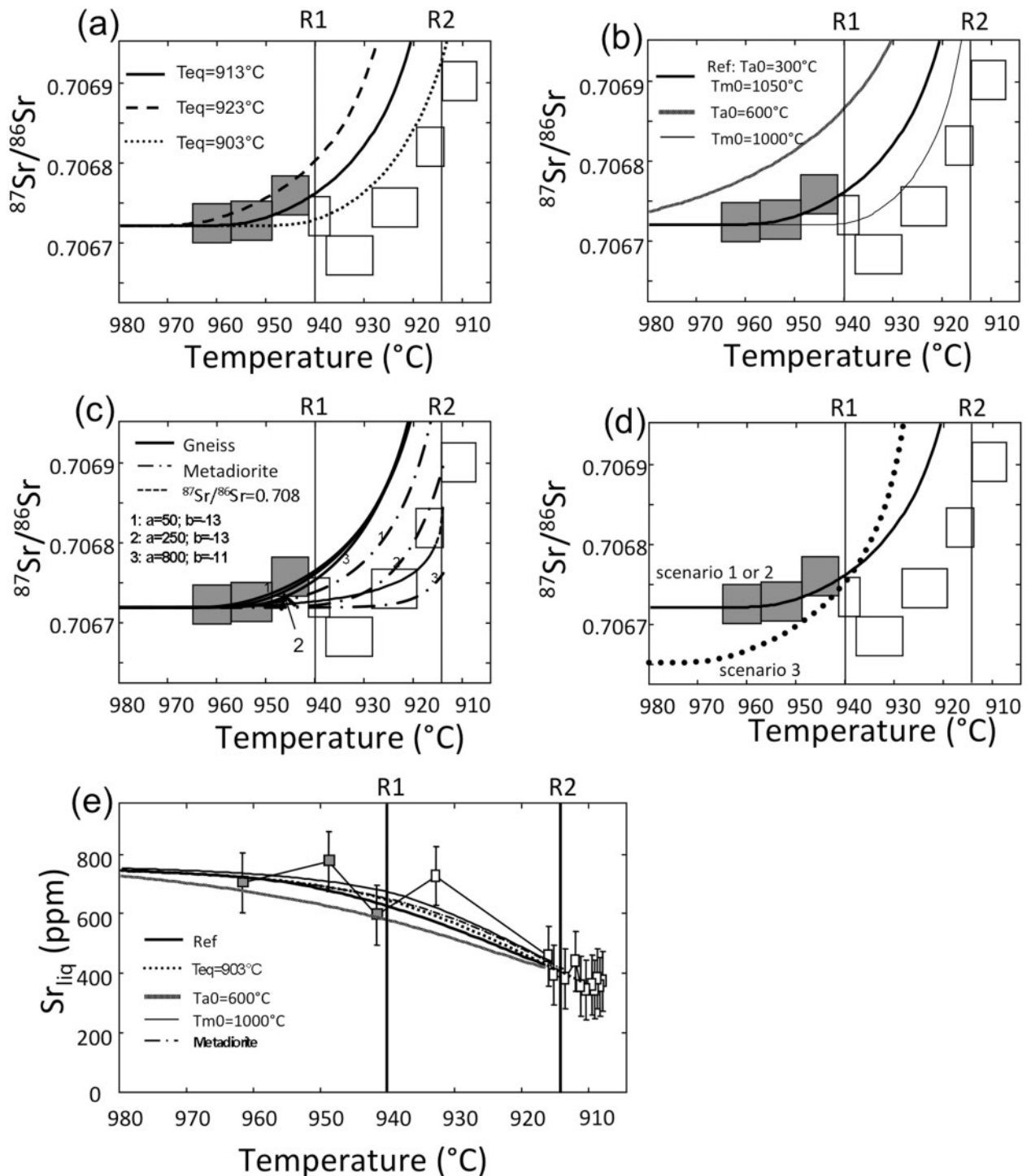
**Fig. 9.** (a–d) Model of the first part of the Sr isotope evolution (zones 6, 7 and 8 in Fig. 8), before recharge (no recharge set in the model) showing the influence of various parameters on Sr isotope evolution in PAR 130. The bold continuous line is the reference case as shown in Table 2 and is the same for all panels. Each curve varies one parameter compared with the reference case. (a) Influence of Teq (magma–wallrock equilibration temperature); (b) influence of starting temperature of the crust (Ta0) and of the magma (Tm0); (c) influence of the crust lithology and melt fraction curve (parameters a and b); (d) influence of the starting isotopic composition of the magma (see text for description of scenarios 1–3). (e) Evolution of Sr concentration in the melt with temperature with the same parameters as in (a)–(d).

ratio of the magma chamber, which is maximized by large volume and/or spherical shape. We will see below how the values of temperature parameters and melt fraction function influence the $Teq_{model}$ and Ma0.

### Effect of temperature

The initial temperature of the melt or of the country rock has a large effect on the Sr isotope curve for a given Teq (Fig. 9b) and therefore on $Teq_{model}$, Ma0 and the final melt fraction in the country rock, fa (Table 4). The percentage of anatectic melt is fairly insensitive to the increase of Ta0 but decreases more significantly with a lower initial magma temperature.

For a low initial temperature of the magma (Tl = 1000°C), $Teq_{model}$ is higher (928°C) and Ma0 lower (0·118) and the amount of anatectic melt is lower (4·5% of the total melt) than in the reference case. For hotter crust (600°C), $Teq_{model}$ is much lower (880°C), implying interaction with a larger portion of the crust, and the percentage of anatectic melt is slightly higher (5·4%).

Overall, the percentage of anatectic melt in the total melt obtained by fitting the data is thus relatively insensitive to the temperature parameters of the model, whereas the amount of crust thermally involved varies significantly. In general, $Teq_{model}$ values seem rather high and Ma0 values low, and might not be realistic, in which case high temperatures (liquidus temperature of the magma or initial temperature of the country rock) will be required to account for the observed contamination. External constraints on Ma0 in the Parinacota system are unfortunately not available.

### Effect of assimilated lithologies

For the gneiss (reference case), with a low liquidus temperature, variations in the a and b parameters of the melt fraction curve as shown in Fig. 7b have little effect on the resulting Sr isotope curve (within analytical uncertainty; Fig. 9c). A less fertile lithology (metadiorite) produces significantly less contamination (all other parameters being equal) and accordingly a higher $Teq_{model}$ (928°C) and lower Ma0 (0·186). The effect of variation in the melt fraction parameters as shown in Fig. 7b is significant in the case of the metadiorite with high liquidus temperature because of the larger temperature interval between liquidus and solidus. Case 1 shown in Fig. 9c has a melting curve actually close to the dacite magma (Fig. 7b), which is unrealistic and represents extreme values of these parameters. However, it may account for intermediate lithologies. The amount of anatectic melt necessary to fit the data is only slightly lower for the more refractory crust (4·2–4·5% of the total melt).

The curve calculated with the augengneiss (not shown) is indistinguishable from that with the metadiorite. In the case of a less radiogenic ($^{87}Sr/^{86}Sr = 0.708$) fertile crust, the contamination is significantly lower (Fig. 9c).

### Effect of starting isotopic ratio

The modelled evolution of isotopic contamination starts with a slow increase of $^{87}Sr/^{86}Sr$ with decreasing temperature, followed by an increase in the slope of the curve. For a starting isotopic ratio of 0·70672 (as used for scenarios 1 and 2) the modelled increase in $^{87}Sr/^{86}Sr$ from 0·70672 to 0·70675, as observed in the inner part of the crystal (Fig. 9d), occurs over about 30°C, $^{87}Sr/^{86}Sr$ remaining constant between the liquidus temperature and 970°C. This is consistent with the observed zone size in the crystal. In contrast, for a starting isotopic ratio of 0·70665 (scenario 3), the same variation of Sr isotopes corresponds to a variation of temperature of 5°C (945°C down to 940°C; Fig. 9d) and an increase in crystal fraction from 4·5 to 6%. This would imply that zones 8 to 6 (200 μm) grew over 5°C, which would be inconsistent with the melt fraction function chosen for the magma and would imply a significantly higher growth rate before than after recharge. A very low Chi (fraction of the anatectic melt mixed with the magma) will slow down the assimilation but not change the shape of the curve, and the same effect would be observed but at lower temperatures. For this reason, we consider the low starting isotopic ratio unlikely. In this case it is not possible to obtain the observed decrease in $^{87}Sr/^{86}Sr$ by recharge with the same magma, and scenario 3 will therefore not be considered further.

## Results (2); EC-E'RAFC modelling, after recharge

The modelled evolution of Sr and $^{87}Sr/^{86}Sr$ in scenarios 1 and 2 using the parameters of the reference case, where Teq is adjusted to fit the data at the rim, is shown in Fig. 10. Both cases allow the observed increase of $^{87}Sr/^{86}Sr$ to 0·707 (value of the groundmass crystals) by temperatures between 910°C and 905°C. Some variation is possible using higher Teq (thermal interaction with a smaller amount of the crust), and Chi < 1 (not all the anatectic melt is mixed). Variations of the recharge temperature (not shown) change the correspondence between temperatures and growth zones, involving a possibly non-linear growth rate of plagioclase crystals. However, with a recharge at 970°C, all other parameters being equal to the reference case, an $^{87}Sr/^{86}Sr$ of 0·707 is reached at 910°C as in the reference case with a similar percentage of assimilated crust (22%). The model is therefore insensitive to the recharge temperature. If the country rock starting temperature is 600°C (not shown), $Teq_{model}$ is lower (870°C) and the amount of assimilated crust slightly higher (25%). With a metadioritic crust, all other parameters being equal to the reference case, the final $^{87}Sr/^{86}Sr$ is 0·70686, significantly lower than the external zone of Pl and the groundmass crystals. This implies that if only metadioritic crust is assimilated, it must occur with higher
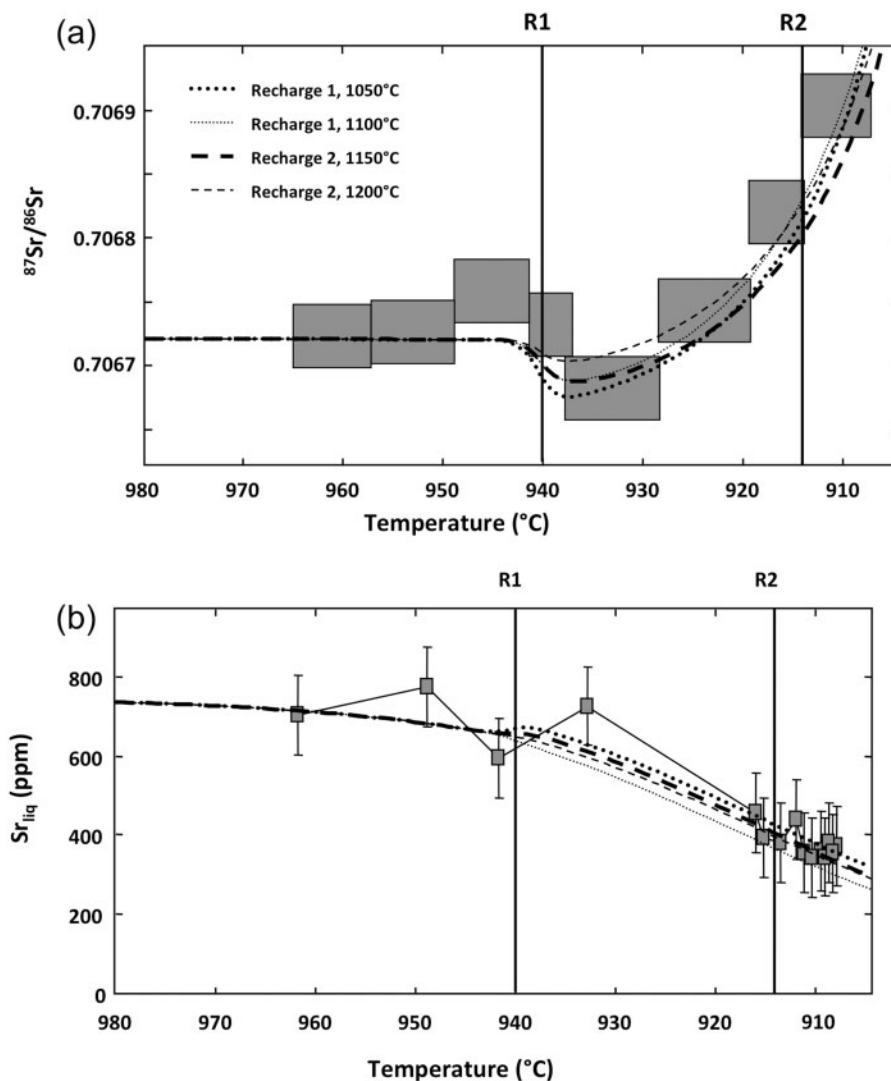
**Fig. 10.** Models of scenarios 1 and 2 including recharge at 940°C. (a) $^{87}Sr/^{86}Sr$ and (b) Sr concentrations vs temperature ($T$). (See the text for discussion.)

temperatures, for instance in the starting country rock. The same is expected with a less radiogenic, magmatic country rock.

The models do not allow the distinction between scenarios 1 and 2. However, the total amount of assimilated crust (gneiss) when the magma reaches 0·7070 is close to 20% for both scenarios, with all chosen temperatures for the recharge magma, and is therefore robust and insensitive to variations of the most unconstrained parameters. The effect of a possibly less radiogenic crust would be to increase the amount of assimilated crust needed and thus make this a minimum estimate.

### Summary of EC-AFC results
The models presented in Fig. 10 show that crystallization, assimilation and recharge can be reasonably quantified

from a texturally correlated core–rim $^{87}Sr/^{86}Sr$ and Sr concentration profile from a single feldspar crystal. The most robust result is that the calculated amount of assimilated crust depends almost entirely on the composition of the crust (Sr content and $^{87}Sr/^{86}Sr$). Thus for PAR 130, 20–25% assimilation is required for a crust similar to the Belén gneisses, more if the crust contains less Sr or is less radiogenic. This significant assimilation is not evident from the bulk-rock data because of the high Sr content of the Parinacota magmas: the bulk-rock Sr isotopic ratio of PAR 130, only slightly higher than that of most Parinacota samples, actually reflects substantial assimilation during crystallization in the magma chamber.

As with any petrogenetic modelling, there are limitations that prevent better constraints on conditions of assimilation such as temperatures or composition. The first

is from the data themselves (the resolution of the sampling and analytical issues such as precision and blanks) but this is negligible compared with the second, which is from the model. The sophistication of the Spera & Bohrson (2004) model means that it deals with a large number of parameters, all of which have uncertainties—some more than others. The analysis above shows that the main uncertainties are in the composition of the contaminant and in the way magmas interact thermally with the crust, represented in the model by Teq and Ma0. These parameters are poorly constrained and the model is highly sensitive to them; therefore, there are many sets of parameters that provide a good fit to the data. On the other hand, the model is less sensitive to parameters such as magma initial and recharge temperature or melt fraction curves and the composition of the starting and recharge magmas (which are also better constrained). Despite these limitations we can be confident that the observed amount of contamination in PAR 130 requires a combination of high temperatures and/or a relatively thermally isolated system (high Teq). Finally, sophisticated though the Spera & Bohrson (2004) model is, it still has limitations in its capacity to quantify recharge and its effects such as reheating and crystal dissolution. Nevertheless, we conclude that realistic quantitative constraints on magma evolution can be extracted from single crystals. This is a significant advance on our original qualitative recognition of processes such as contamination and recharge in crystal profiles (Davidson & Tepley, 1997).

## MAGMA EVOLUTION AT PARINACOTA: DISCUSSION
### Crystal zoning and magma history

From the chemical and Sr isotope zoning analysed in crystals we can infer an evolution of the melt in contact with these crystals during their growth, but how representative is this of the magma history? The question is important in any crystal zoning study, but is more acute in the case of Sr isotopic microsampling because the method is time consuming and the total number of analyses is necessarily limited. The question needs to be considered at three scales: within crystals, within the plagioclase population, and between all mineral phases. The answer will depend on the characteristics of each sample. In some samples the average of our microsampling data does not seem to be consistent with the whole-rock isotopic ratios: in PAR 084 and PAR 082, the whole-rock data are as low as those of the least radiogenic zones analysed. This implies either that these zones are quantitatively representative of the sample and the amount of Sr in the other zones is negligible or that some unradiogenic Sr present in the rock has not been sampled (or a combination of both).

### Crystal scale
The first point to consider is, at the crystal scale, how well do the measured profiles reflect the melt in equilibrium with the growing crystal? The accuracy of the melt evolution inferred from zoning depends both on the spatial resolution of the sampling methods and on the width of the zones of distinct composition. The spatial resolution of chemical analyses varies with the method but is in general better (especially with electron microprobe) than for microdrilling. The spatial resolution of Sr isotopic microsampling can be as good as $50 \, \mu m$ width (Charlier et al., 2006), provided that the concentration is high and/or the length of the zone is sufficient to allow sampling of a sufficient amount of Sr. Further complications, such as zone obliquity relative to the section (causing different zones to be intersected with depth) or the difficulty of following curved growth zones precisely, will decrease the spatial resolution of the profile, on length scales similar to the minimal zone width measured ($50 \, \mu m$) and result in a measured profile that is smoother than the actual melt evolution.

The amount of Sr needed to characterize each zone in turn depends on the precision needed and therefore on the isotopic contrast between zones. Ideal conditions to reflect best the magma evolution are large, Sr-rich crystals, with large zones of contrasting isotopic composition, reflecting high crystal growth rate compared with time scales of variation in magma composition. In this respect, PAR 130 Pl allows a good characterization of contamination because of its relatively simple history, one recharge and limited dissolution of the crystal resulting in concentrically zoned, large crystals, as well as significant increase in isotopic ratio towards the rim. In contrast, samples such as PAR 084 and PAR 068, where several recharge events occur and growth zones between resorption surface are small, are likely to record incompletely the melt history and some events may be too small to be analysed confidently. In some small zones such as in PAR 068, breakage of adjacent zones also may generate mixed signals. In any case, any observed isotopic variation provides useful information on the melt history, and chemical zoning and microtextures are important to assess how much of this history might be missing.

### Plagioclase populations
Even if Sr microdrilling succeeds in sampling representative zones within a crystal, the recorded melt evolution is that of a specific crystal and represents one real history that may not be the history of the whole magma system. This can be partly evaluated by comparing several plagioclase crystals in the same sample and distinguishing populations with common characteristics (Martin et al., 2010). A careful preliminary study of chemical zoning allows the identification of crystal types that share supposedly a

common history or part of it. This includes the recognition of xenocrysts (from unrelated country rock), antecrysts (from earlier possibly solidified stages of the magma system) and 'true phenocrysts', which may again be divided into various types having a distinct history if grown from several successive batches of recharge magma each containing crystal cores. The number of crystals that is necessary to reflect the crystal population is a way to account for the complexity of the population and of the magma history (Wallace & Bergantz, 2005). In the same way, the fact that Sr isotopic zoning of a crystal does not seem to be representative of the sample, as for 084 and 082, is itself a characteristic of the sample and reflects its complex history. We examine below how representative the drilled crystals are for each sample.

In PAR 130, three zoning types have been sampled. With only one complete Type I (large oscillatory zoned) crystal drilled, we cannot rule out some variations in isotopic profile, especially in the core, although chemical zoning is very consistent between Type I crystals (Ginibre *et al.*, 2002). By contrast, the core of a Type IIa (resorbed low-Sr core) crystal is consistent in isotopic ratio with the corresponding zone (R2) of the Type I crystal. Some variation is seen in the two high-Sr cores (Type IIb), which is consistent with chemical variations between these cores. Overall, although some variation may occur in detail, we are confident that we sampled representative zones of the crystal population of PAR 130. An exact mass balance would require a detailed crystal size distribution (CSD) study (see Morgan *et al.*, 2007). However, the new whole-rock $^{87}Sr/^{86}Sr$ determination (Fig. 5) lies within the range of values obtained for microdrilled zones from plagioclase containing the bulk of the Sr inventory.

For PAR 165, the chemical zoning is straightforward and we drilled only one sample. The whole-rock Sr isotopic ratio is intermediate between core and rim isotopic ratios in plagioclase and there is no indication that the feldspar history is not representative of the whole sample. In PAR 084 the chemical zoning patterns also seem consistent between crystals, with three well-defined zone compositions, even if not all three zones are present in all crystals. However, the low whole-rock isotopic ratio compared with the microdrilled data suggests that some unradiogenic Sr has not been sampled. In this sample, the high-Sr parts of the plagioclase crystals, which are more likely to be unradiogenic, are thin rims that are difficult to sample and cores that are not present in each crystal but are, in some cases, large. Therefore the missing unradiogenic Sr may be present in other plagioclase crystals. Alternatively, as discussed in the next section, it may be present in other minerals not sampled in this study, which focused on plagioclase feldspar.

For PAR 082 a number of crystals have been analysed and are representative of the chemical zoning. Indeed,

plagioclase cores that are close chemically (P4, P5, Pl, P0) have similar isotopic ratios, whereas the high-Sr core is less radiogenic. Plagioclase rims are close isotopically to the groundmass. However, as in PAR 084, some unradiogenic Sr is missing in our analyses. This may be partly due to unsampled unradiogenic plagioclase cores. However, the low modal abundance of feldspars (5%) and the small contrast in Sr concentration and $^{87}Sr/^{86}Sr$ between feldspar and groundmass make this influence small. Mass-balance calculation of a maximum effect of high-Sr feldspar, assuming 7% feldspar, which is a high estimate, and with only high-Sr compositions such as the core of crystal Pl3, gives a whole-rock isotopic ratio of 0·706694, close to, but still slightly higher than, the measured whole-rock $^{87}Sr/^{86}Sr$, 0·706678 ± 9. A more realistic estimate of the amount of high-Sr plagioclase cores, which are relatively rare in this sample, is therefore unable to account for the low whole-rock isotopic ratio. In this case, other mineral(s) must be considered.

In PAR 219, both types of plagioclase crystals (Pl, isolated patchy zoned; P2, clustered with high-Sr cores) appear to be antecrysts, based on the thin sieve-textured calcic rims with higher Fe and Mg concentrations. Whether the two types have a common or different origin is less clear because the patchy zoned rims in clusters and the whole patchy zoned isolated crystals are similar chemically and isotopically, although morphologically different. They may have grown from similar or related magmas in physically separate environments. Likewise, although the groundmass melt is significantly more mafic, the Sr content and isotope ratios are close to those recorded by the patchy zones of the plagioclase and it is not clear whether plagioclase records similar magmas from earlier distinct histories or is more directly related to the groundmass magma. In PAR 068, the chemical variations between cores and the small size of zones, making them difficult to sample, imply that probably only part of the magma history is represented in the two drilled crystals.

### Mineral assemblage

Although plagioclase is generally the main Sr-bearing phase, it may not be the only one. Some missing Sr might be in other phases, where other parts of the history may be recorded. This is probably the case in the andesite PAR 082, where feldspars, with chemical compositions typical for rhyodacites and sieve-textured calcic rims, can be considered as antecrysts, and do not account for the whole-rock Sr isotope budget. In this sample apatite abundance, both as inclusions in mafic minerals (≪1%) and in the groundmass, is small so that its Sr contribution is believed to be negligible. Amphibole and pyroxene are found in feldspar-free clusters, which suggests that they were introduced by a feldspar-free mafic magma. Using partition coefficients of 0·46 for amphibole and 0·06 for pyroxene, 10% amphibole and 5% clinopyroxene in equilibrium

with PAR 011 (Upper Ajata) can account for the discrepancy between whole-rock and groundmass. Therefore, the Sr isotopic ratio measured in feldspar in this sample reflects only part of the magma history. In such cases the whole history would require isotopic studies of other phases.

In PAR 130, PAR 084, PAR 068, PAR 165 and PAR 219, plagioclase is commonly observed in clusters associated with pyroxene, which is the main other mineral and is likely to be representative of at least part of the magma evolution. Therefore, in these rocks, plagioclase and pyroxene seem to have a common history, although different populations of pyroxenes may also exist. Rounded biotite in PAR 130 might come from a more contaminated part of the magma system (country rock or antecrysts) and contribute to the high whole-rock isotopic ratio compared with the highest $^{87}Sr/^{86}Sr$ found in plagioclase. In PAR 084, pyroxene crystals not associated with plagioclase in clusters may have different histories. Large apatite crystals (up to 100 μm) occur in the groundmass, in pyroxene clusters and in small isolated pyroxene crystals and, given their high Sr content, may play a role in the low-Sr whole-rock Sr isotopic ratio.

In all cases, detailed isotopic studies of all phases can only make the reconstructed magma history more complete, especially in samples where this history appears to be complex.

### Magma evolution from combined chemical and isotopic zoning data

Isotopic zoning data are useful for the identification of contamination and recharge processes, especially if the relationships between components are simple, such as repetitive recharge with a similar mafic magma and assimilation of a radiogenic crust. However, the processes affecting the magma chemical and isotopic composition may be more complex and Davidson *et al.* (2007) emphasized the importance of combining petrological studies with isotopic profiles. In our study, the trace element zoning data are critical to the interpretation of zoning profiles because of the presence at Parinacota of at least two distinct mafic magmas. The comparison of our study with that of Davidson *et al.* (2007) (Fig. 11) shows that similar looking $^{87}Sr/^{86}Sr$ profiles can have very different interpretations if chemical zoning is taken into account. In PAR 084, isotopes alone would not necessarily allow the identification of the two recharge magmas, but might suggest assimilation followed by mafic recharge. In PAR 082, the slight decrease in isotope ratio alone does not illustrate the profoundly different nature of the resident and recharge magma. Only the comparison of isotopic zoning with textures and chemical zoning allows us to distinguish mixing of contrasting end-members from assimilation–recharge. We suggest that such an approach can be useful in any volcanic system. The occurrence of several types of mafic

magmas such as at Parinacota is not an exception and can be easily overlooked if trace element concentrations are not combined with Sr isotopic data.

## Assimilation and mixing history at Parinacota
### Composition of the mafic magmas

Like most CVZ volcanic products, all Parinacota samples have Sr isotopic compositions that are higher than most oceanic mantle values. The commonly accepted explanation is the ponding and differentiation in the lower crust [melting, assimilation, storage and homogenization (MASH) zones; Hildreth & Moorbath, 1988] of primitive arc magmas to form radiogenic basaltic andesites with a baseline isotopic signature by fractional crystallization and crustal assimilation. Annen *et al.* (2006) showed that the compositions of major and trace elements and isotopes of intermediate to silicic magmas equilibrated in these hot zones depend on various parameters such as the level in the crust, lithology, injection rate and time since onset of basalt injection. These hot zones can therefore simultaneously produce a large variety of mafic to intermediate magmas that can then be mixed. Further contamination in the upper crust may be superimposed on the lower crust history and further increase the diversity of erupted compositions.

At Parinacota, Upper Ajata (high Sr and Ba concentrations, $^{230}Th$ excess, high Sr/Y, Dy/Yb, low $^{87}Sr/^{86}Sr$) and Lower Ajata (lower Sr and Ba concentrations, U excess, low Sr/Y, low Dy/Yb, higher $^{87}Sr/^{86}Sr$) basaltic andesites form two mafic compositional end-members. The Ajata lavas are younger than most of the other samples and can therefore not be involved directly as parents of older samples; however, earlier formed Ajata-like magmas may be involved. Decoupling between Sr concentrations and isotopes recorded in plagioclase reflects the diversity of magmas present in Parinacota's evolution. This diversity can be viewed as caused by mixing between two end-members similar to the Upper and Lower Ajata magmas and further crustal assimilation at various levels, or by a range of parent magmas formed in the hot zone, with intermediate characteristics.

In fact, no Upper Ajata-like plagioclase cores are found in any of our samples to document an origin from Ajata-like magma. However, the Upper Ajata magma was not saturated in plagioclase and its high Sr content reflects evolution largely in a plagioclase-free environment. High Dy/Yb and Th excess suggest evolution in, and assimilation of, mafic crust with residual garnet (Mamani *et al.*, 2008; Hora *et al.*, 2009). If the high-Sr concentrations in other Parinacota samples come from an Ajata-like magma, this will not be documented in plagioclase, and the lowest $^{87}Sr/^{86}Sr$ recorded will be that at the onset of plagioclase crystallization. Likewise, the Lower Ajata-
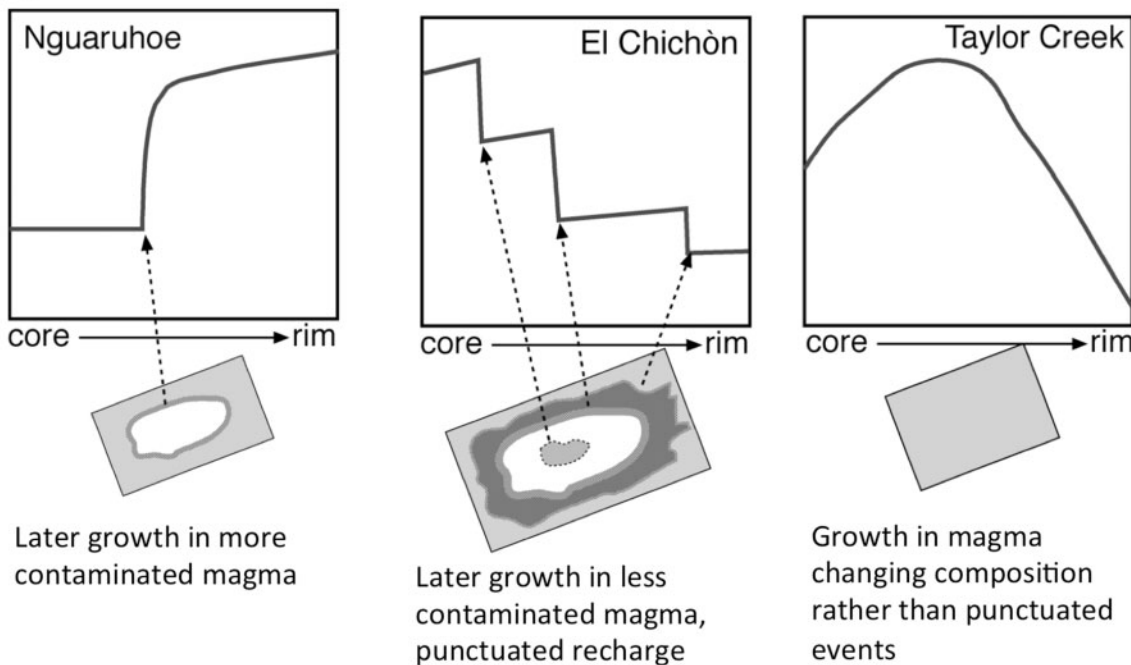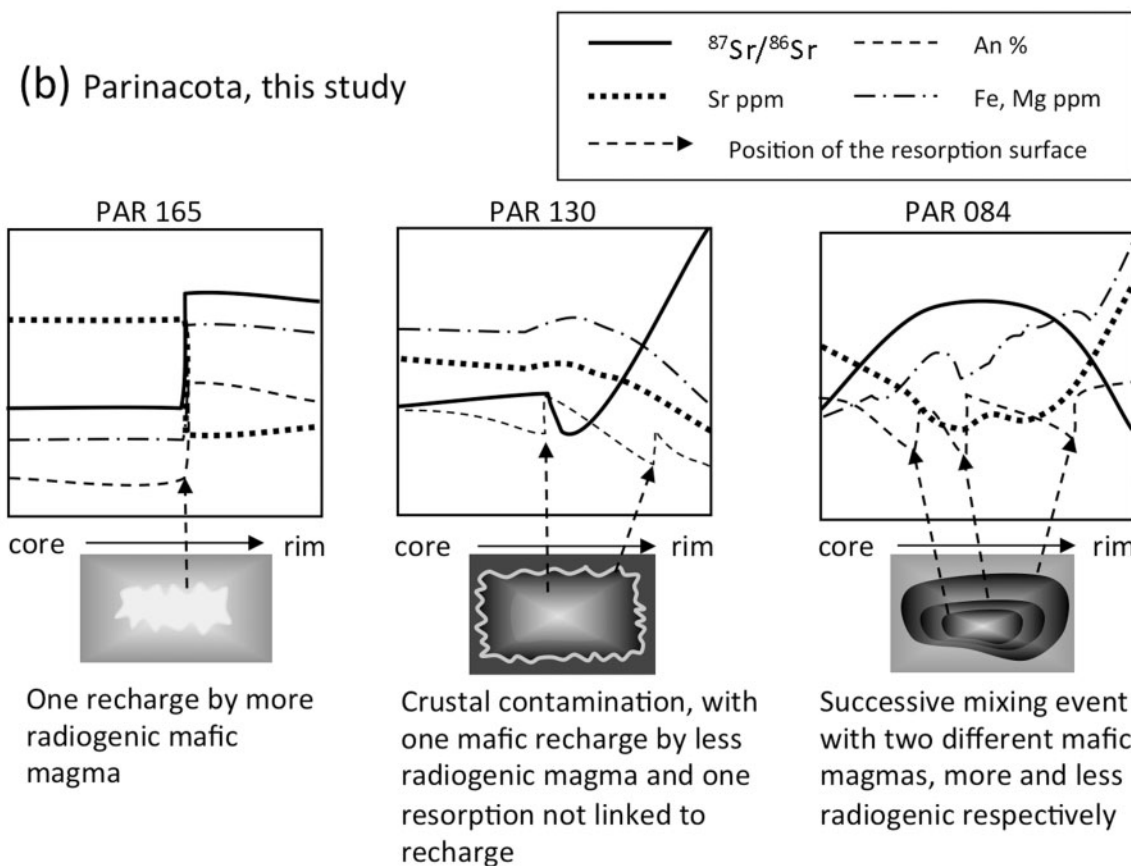
**Fig. 11.** Comparison of schematic Sr isotopic profile types from Davidson *et al.* (2007) and from this study. The chemical zoning information allows us to relate the magma evolution not only to assimilation or contamination but also to magma chemical composition.

(continued)

type end-member is also plagioclase-free because plagioclase crystals in PAR 219 are clearly antecrysts with a lower Sr isotopic ratio and sieve-textured calcic rims. The only analysed plagioclase zones that may be related to Lower Ajata-type magmas are thus plagioclase rims in PAR 165 and intermediate zones in PAR 084. In both cases, they are grown after plagioclase resorption from the mixture of the recharge magma with the resident magma. The low Sr concentration of PAR 219 suggests that plagioclase has played a role in its evolution; however, this early history is not documented in the erupted product, possibly because plagioclase cores, which crystallized at depth in water-undersaturated conditions, dissolved upon decompression.

*Plagioclase core compositions.* We have shown that the lowest $^{87}Sr/^{86}Sr$ recovered from plagioclase is not the lowest in the system (Lower Ajata sample PAR 011), suggesting that some contamination has always occurred before plagioclase crystallization even began. Although the earliest history of the mafic magma may not be recorded in plagioclase, the plagioclase cores and zones surrounding recharge-induced resorption horizons can still provide invaluable insights into the sources of the mafic magmas. We first focus on the crystal cores of the entire sample suite, showing $^{87}Sr/^{86}Sr$ against the average Sr equilibrium melt concentration, assuming instantaneous equilibrium between the melt and crystal core (Fig. 12). The isotopic ratio chosen for the high-Sr core of PAR 219 (0·70655) is that of the least radiogenic zone, corrected for glass contamination during drilling.

We distinguish several groups of cores (Fig. 12). Sr-rich cores from PAR 130, PAR 219 and PAR 165 are similar and have the lowest $^{87}Sr/^{86}Sr$, although An, Fe, Mg (not shown; see Ginibre & Wörner, 2007) are higher in PAR 165 core ($An_{48-60}$, 3500–4000 ppm and 300 ppm respectively) than in the other two ($An_{40-55}$, 2500–3000 ppm, 100–200 ppm). Between 0·70665 and 0·70672, we observe both low-Sr cores (PAR 068 and PAR 130 Type I), also similar in terms of Mg, Fe and An content (not shown; see Ginibre & Wörner, 2007), and high-Sr cores (PAR 068-P9 and PAR 082-P13, but the latter has significantly lower Fe and Mg contents). PAR 084 core has the highest Sr concentration and isotopic ratio, which is closest to PAR 082 groundmass (but lower in Fe and Mg contents). PAR 082 cores, except P13, form a distinct group with
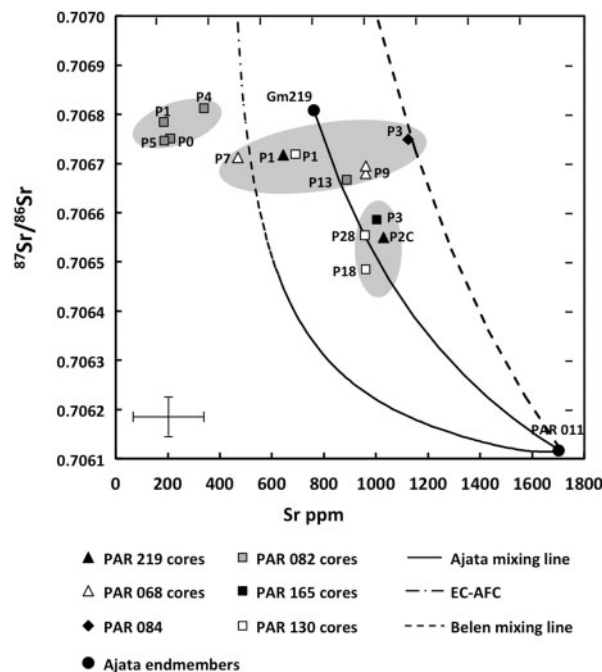


**Fig. 12.** Measured $^{87}Sr/^{86}Sr$ vs calculated Sr concentration in the melt for all crystal cores. Shaded areas show three compositional groups: high-Sr cores of PAR 165, PAR 130 and PAR 219 are the least radiogenic and lie close to the mixing line between Ajata end-members (PAR 011 and PAR 219 groundmass); most PAR 082 cores form a distinct low-Sr radiogenic group; all other cores have variable Sr contents at similar $^{87}Sr/^{86}Sr$ and lie mostly between a simple mixing curve of PAR 011 with Belén Gneiss and an EC-AFC curve for PAR 11 at upper crustal conditions ($D_{Sr}>1$).

lower Sr content, reflecting a significantly more felsic magma. All core compositions, except for PAR 082, lie close (mostly within the error of $Sr_{melt}$ concentration) to the mixing line between the two Ajata end-members. The scatter is larger at $^{87}Sr/^{86}Sr > 0·70665$, suggesting a different origin and/or evolution path. All core data except for PAR 082 also fall between the simple mixing line of PAR 011 with Belén crust and one EC-AFC path of PAR 011 in the upper crust (plagioclase present). By adjusting the lithology (Sr concentration, partition coefficient and isotopic ratio), an EC-AFC path can be found for any core composition, including those on the mixing line between Ajata-like magmas, and thus the two processes cannot be easily distinguished. The group of high-Sr cores (PAR 165, PAR

**Fig. 11.** Continued

PAR 165 $^{87}Sr/^{86}Sr$ profile is similar to that of Nguaruhoe. However, in the latter case, the more contaminated magma is also more felsic, whereas the recharge magma in PAR 165 is more mafic, as shown by the increase in Fe and Mg content, although Sr-poor and more contaminated. In PAR 130, the minor and trace elements variations are distinct for two different dissolution surfaces, and allow us to explain why Sr isotopes behave differently, in contrast to cases such as El Chichon, where each dissolution surface represents a recharge event with a similar less-contaminated magma. In PAR 084, recharge events with two different mafic magmas result in an isotopic profile similar to first contamination followed by progressive unradiogenic recharge as in Taylor Creek feldspars. Dissolution surfaces help us to identify punctuated recharge events confidently, which may otherwise be difficult to distinguish from more gradual recharge or contamination steps owing to the resolution of the microdrilling.

219 and PAR 130) lies on the Ajata mixing line, whereas the cores of PAR 68-P7 and PAR 130-Pl, with less Sr at a given $^{87}$Sr/$^{86}$Sr, suggest more fractionation, and the cores of PAR 68-P9 and PAR 084 P3 indicate more contamination with limited decrease of Sr concentration. Analyses of earlier crystallizing phases would be necessary to help distinguish the two possibilities. Overall, core compositions reflect a complex combination of variable parental magmas, possibly variable proportions of different mafic end-members, and additional contamination processes. More precise Sr concentration analyses (with *in situ* methods such as laser ablation inductively coupled plasma mass spectrometry rather than electron microprobe) could also allow a better distinction between paths.

*Recharge magma compositions.* Recharge events may provide more information on the mafic magmas than the cores because compositions both before and after recharge are recorded in plagioclase zones. Low-Sr recharge events are recorded in PAR 165 rims and in PAR 084 second zone (Fig. 13a and b). In PAR 165, the $^{87}$Sr/$^{86}$Sr, An, Mg and Fe contents of plagioclase rims are close to those of PAR 219 groundmass crystals. The contrast between the melt in equilibrium with the core or the rim of PAR 165 plagioclase and PAR 219 groundmass is smaller than the uncertainty on Sr concentration in the melt. Therefore simple mixing with PAR 219 groundmass cannot be distinguished from additional contamination. For the first (low-Sr) recharge event of PAR 084, a mixing line between the liquid in equilibrium with the core drilled zone (zone 6) and a low-Sr mafic magma should be able to produce liquids in equilibrium with the intermediate zone of the crystal (drilled zones 4 and 5). The mixing lines (Fig. 13b) show that the groundmass of PAR 219 as low-Sr recharge magma is slightly too unradiogenic to fit the data and that a small amount of contamination is required. Furthermore, the melt after recharge has much lower Fe and Mg concentrations than PAR 219 groundmass (not shown; Ginibre & Wörner, 2007). This may indicate a more evolved recharge magma, or only a small amount of the recharge magma, which only slightly changes the composition of the resident magma.

High-Sr recharge events are recorded in PAR 084 (Fig. 13b) and PAR 082 (Fig. 14). In the case of PAR 084, the composition of external zones can be explained by mixing with Upper Ajata-like magma and further crustal assimilation is not required, although such assimilation may have occurred and not be identified if the EC-AFC path is close to the mixing line. In fact, this mixing line is close to the evolution path of PAR 130 TI and PAR 068 P7 cores (Fig. 12).

In contrast to PAR 084, PAR 082 rims are almost as radiogenic as the cores, which is not consistent with an unradiogenic recharge such as PAR 011. In this sample, the large compositional contrast between the resident
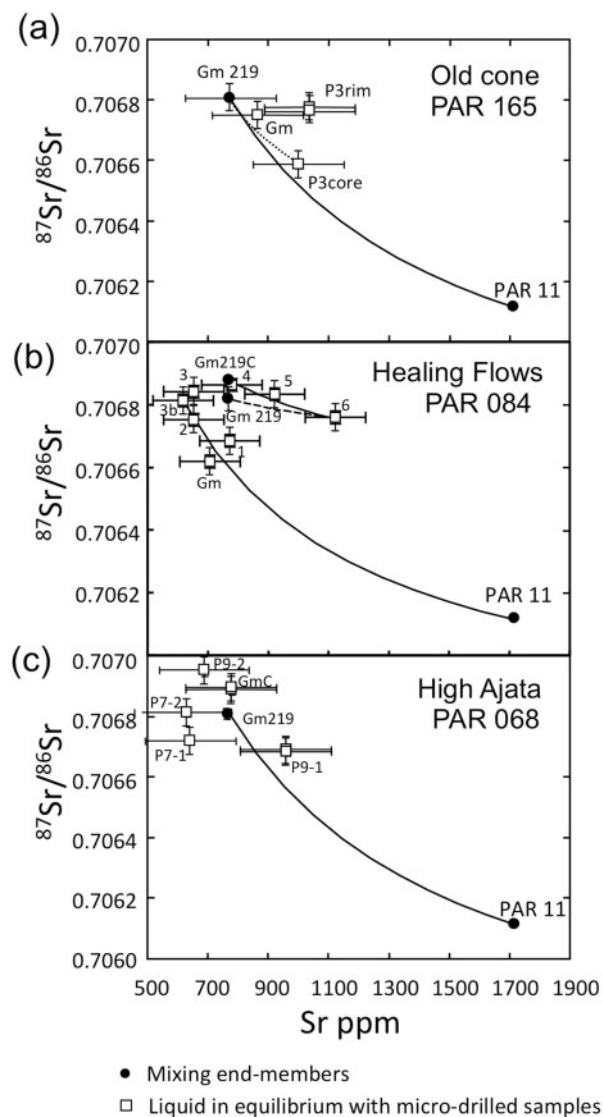


**Fig. 13.** $^{87}$Sr/$^{86}$Sr vs Sr concentration for single samples representing the three main stratigraphic groups: (a) PAR 165; (b) PAR 084; (c) PAR 068. Open squares are calculated liquids in equilibrium with the various zones of plagioclase (see Figs. 2–5 and Table 1); drilled zone numbers are indicated. Filled circles represent possible mixing end-members. Gm, groundmass; GmC, groundmass crystals; Gm 219C, groundmass of PAR 219 contaminated with crust. The amount of contamination is chosen arbitrarily to fit the plagioclase data.

magma (rhyodacitic) and the recharge magma (basaltic andesite to andesite) allows an estimation of the proportion of the different mixing components. As shown by Ginibre & Wörner (2007), the observed PAR 082 sample can be considered as a mixture of ∼40% of differentiated rhyolite from the Rhyolite Domes or unerupted equivalent (300–400 ppm Sr) with around 60% of basaltic andesite with ∼1500 ppm Sr (Fig. 15). Alternatively, a high-Sr andesite close in composition to PAR 082, possibly derived from PAR 011 by fractional crystallization, could have entrained
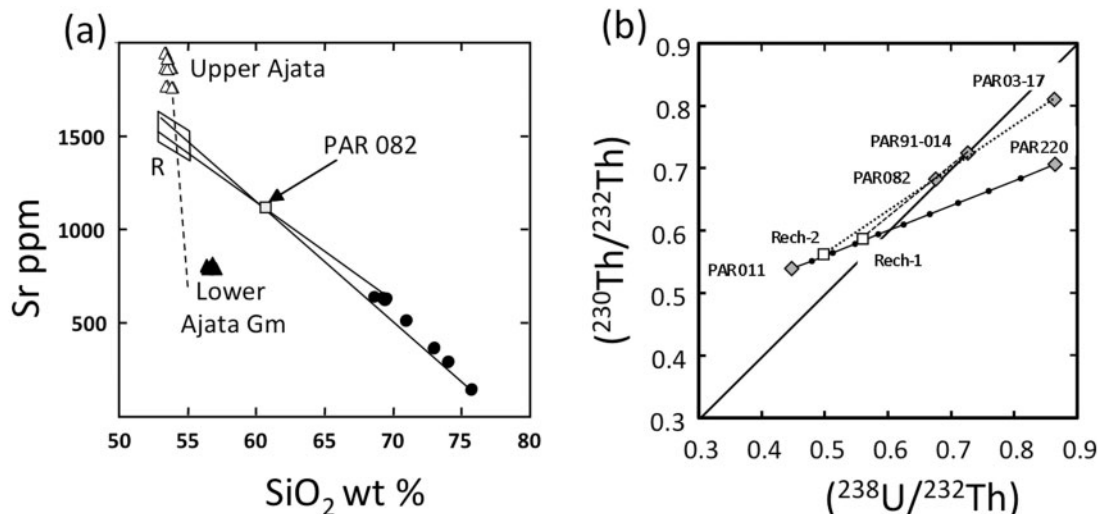
**Fig. 14.** (a) Likely composition of the PAR 082 recharge magma (R) in a plot of Sr–SiO$_2$. (b) U–Th diagram showing Parinacota data [PAR 082, PAR 011, PAR 220 similar to 219 and rhyolite PAR 91-014 from Bourdon *et al.* (2000); PAR 03-17 rhyolite from Hora *et al.* (2009)], and mixing lines between Upper and Lower Ajata magmas and between rhyolite compositions and a recharge magma to produce PAR 082. Both recharge magmas are chosen to lie on the mixing line between the Ajata end-member magmas. Rech-1 corresponds to mixing (recharge) with rhyolite PAR 91-014, and Rech-2 to mixing (recharge) with PAR-03-17, which has the highest $^{238}$U/$^{232}$Th.
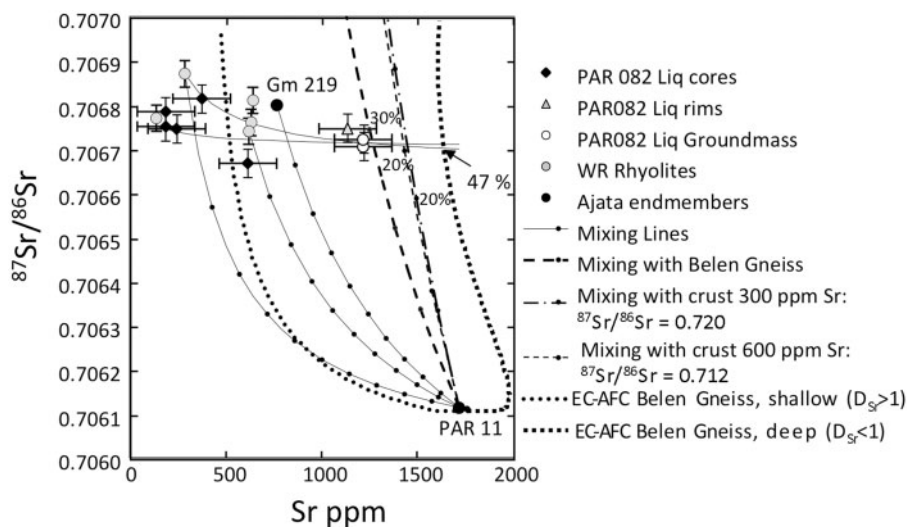


**Fig. 15.** Mixing scenarios for PAR 082 assuming that contamination occurs before recharge. Direct mixing curves with various compositions of rhyolite and of assimilated crust, as well as EC-AFC models with Belén gneiss at depth and near the surface are shown. Percentages refer to the amount of assimilated crust: 30 and 20% points are shown on the mixing lines, and 47% is the amount of assimilated crust in the deep EC-AFC model for a final isotopic ratio of $^{87}$Sr/$^{86}$Sr = 0·70667. It should be noted that the rhyolite compositions shown are whole-rock compositions. The (feldspar-free) melt that is in reality mixed with the mafic recharge magma to form PAR 082 groundmass is likely to have a significantly lower Sr concentration and possibly slightly higher $^{87}$Sr/$^{86}$Sr, depending on the amount and composition of feldspars in the rhyolite. However, the diversity of compositions shown should account for such possible variations.

rhyolitic xenocrysts, but this scenario is less likely for textural reasons (Ginibre & Wörner, 2007). Based on chemical compositions such as Sr and SiO$_2$ (Fig. 14a), if the recharge magma is close to PAR 011 it must, however, have a slightly lower Sr concentration to fall on a mixing line with PAR 082 and the Rhyolite Domes composition. A mixture of 80–75% Upper Ajata and 20–25% Lower Ajata has an

appropriate composition. This estimate is consistent with available U–Th data (Bourdon *et al.*, 2000; Hora *et al.*, 2009). In the U–Th diagram (Fig. 14b) a mixture of 70–80% Upper Ajata and 30–20% Lower Ajata is consistent with the rhyolite compositions (depending on the rhyolite chosen) and PAR 082. However, Sr isotope ratios (Fig. 15) are not consistent with only mixing of these three

components because the recharge mixture mentioned above would have a $^{87}Sr/^{86}Sr$ of 0·706178. Mixing of such a recharge magma with the rhyolites cannot explain the isotopic composition of the plagioclase rims. For a simple mixing model between the rhyolite and a contaminated recharge magma, the recharge magma needs to be almost as radiogenic as PAR 082, significantly higher than calculated above from mixing Upper and Lower Ajata magmas.

We consider several contamination scenarios of pure PAR 011 to arrive at a plausible recharge magma (Fig. 15). If mixing with a Lower Ajata-type magma, as considered above, occurs before or after contamination, it will slightly decrease the amount of contamination needed. Because of the high Sr concentration of PAR 011, simple mixing between PAR 011 and the basement produces enough contamination only if either a large amount of crust or a crust with a high isotopic contrast with the magma is involved. For crust similar to the Belén gneisses, 33% assimilation is necessary to obtain a suitable isotopic ratio for the recharge magma and the Sr concentration of the recharge magma is then more similar to that of PAR 082 than that of the postulated basaltic andesite. Contamination by other lithologies, not exposed around Parinacota volcano but possibly present at depth, may provide an adequate recharge magma (1500 ppm Sr, $^{87}Sr/^{86}Sr$ 0·70668): with 300 ppm Sr and an isotopic ratio 0·720, 20% assimilation is needed, whereas with 600 ppm Sr and an isotopic ratio of 0·712, 24% assimilation is needed. In the U–Th system, contamination with lower crust lying on the equiline at low ($^{230}Th/^{232}Th$) (Hora et al., 2009) also allows for a recharge magma that can mix with the rhyolite to form PAR 082 (Fig. 14b).

Fractional crystallization during upper crustal assimilation (calculated with the EC-AFC model under conditions similar to those used for PAR 130) decreases the Sr concentration of the magma. When the magma then reaches the observed isotopic ratio, its Sr concentration is around 500 ppm, and the magma is then no longer a high-Sr recharge magma. On the other hand, EC-AFC at lower crustal conditions (i.e. without fractionation of plagioclase) will increase the concentration of Sr in the magma (with low $^{87}Sr/^{86}Sr$) and weaken the effect of assimilation on $^{87}Sr/^{86}Sr$. A calculation shown on the diagram for lower crust EC-AFC involves 47% of anatectic melt for the required $^{87}Sr/^{86}Sr$ (0·7067). The resulting recharge magma is then an andesite rather than a basaltic andesite. Disequilibrium melting of the crust may involve preferentially old, high-Rb phases such as biotite (dehydration melting), which provides more radiogenic Sr and allows more effective contamination (e.g. Hammouda et al., 1996; Knesel & Davidson, 1996). However, this effect will be significant only if the $^{87}Sr/^{86}Sr$ of the biotite is extremely high, because of the typically low Sr content of this mineral.

These various models suggest that several sets of conditions of mixing and assimilation may allow the production of a suitable recharge magma for PAR 082, probably involving lower crust conditions, a high-Sr melt and a certain amount of crustal assimilation; however, these models are not well constrained. From plagioclase isotopic zoning it is not possible to distinguish between a contaminated Ajata-like magma and magma from a higher level hot zone that would have acquired a different Sr isotopic signature directly from a basalt. A more complex scenario involving different levels in the hot zone, polybaric crustal assimilation, and mixing of several variously contaminated magmas is also possible. This is consistent with the decoupling observed between Sr concentration and $^{87}Sr/^{86}Sr$ and U–Th isotopes. It is therefore more likely that distinct magma batches acquired their various chemical and isotopic characteristics independently over time rather than being a simple 'instantaneous' mixture of two end-members. Such an early history may have been recorded in other phases such as olivine, pyroxene and amphibole in PAR 082, possibly reflecting the history of the plagioclase-free recharge magma.

PAR 068 whole-rock and plagioclase rims are more radiogenic than any considered mafic end-member. The mafic recharge magmas are difficult to identify in PAR 068 because of the small magnitude of the chemical variations (Fig. 13c), but either they are contaminated as discussed above for PAR 082, or the emplacement and recharge event causes crustal assimilation as discussed below.

### Chronology of mixing and contamination from comparison between cores and rims

Contamination may occur at depth, giving rise to a diverse suite of parental magmas, including the Lower and Upper Ajata-type magmas, and may be followed by only mixing and fractionation at shallower levels in the system, as discussed above. In this case the isotopic diversity is a function of deep 'hot zone' processes. Alternatively, the isotopic diversity inherited from the hot zone may be further enhanced or otherwise modified by shallow-level contamination. At Parinacota, several zones, in particular plagioclase rims and groundmass, as well as some whole-rock samples (PAR 130, PAR 068), have higher isotopic ratios than expected from mixing between the two identified Ajata-type mafic end-members and a rhyolitic one. Early contamination of these end-members before mixing and emplacement has been discussed above. We now discuss the alternative (or additional) scenario in which crustal assimilation is enhanced after recharge with an unradiogenic mafic magma and then recorded in plagioclase rims and groundmass.

We know that assimilation after emplacement and recharge occurs at Parinacota because it is recorded in PAR 130 from the core to the rim of a large crystal (Pl). The

same may have occurred in other samples but may be incompletely recorded in plagioclase. If similar assimilation occurs during dissolution of plagioclase or further growth with a small growth rate, it may be recorded in zones smaller than the spatial resolution of microdrilling and thus be indistinguishable from recharge with an already contaminated mafic magma. This effect can be expected in particular in cases of hot mafic recharge such as PAR 082, PAR 084 and PAR 068. In PAR 084, as shown above, no indication of contamination is related to the high-Sr recharge, although the contamination may be present but similar to the mixing trend. We focus below on PAR 082, although a similar process is possible to explain the high isotopic ratios of PAR 068 rims (higher than in the Lower Ajata end-member). For PAR 082, Fig. 16 shows possible evolution paths in the case where mixing occurs between a rhyolite and a basaltic andesite close in composition to PAR 011, followed by crustal contamination with Belén gneisses (simple mixing). We chose two extreme compositions for the rhyolite (Rh1 and Rh2). Three recharge magmas are considered at 1550 ppm Sr: Rfc results from fractional crystallization of PAR 011 and has thus the same isotopic ratio
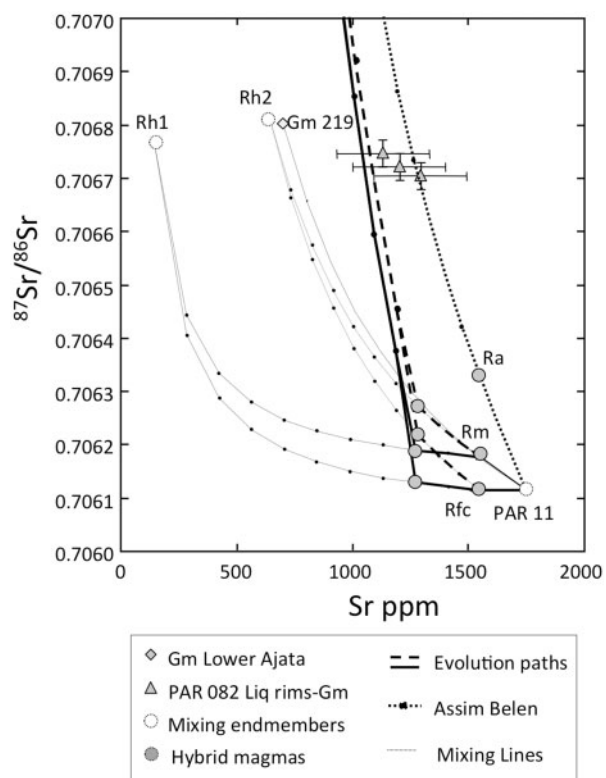


**Fig. 16.** Mixing and subsequent assimilation scenarios for PAR 082, assuming that contamination occurs after recharge: Ra, Rm and Rfc result respectively from crustal contamination, mixing with PAR 219 groundmass and fractional crystallization of PAR 011. These are then mixed with the rhyolite end-members and contaminated (simple mixing) with Belén gneisses.

but lower Sr content, Rm results from the mixing with a Lower Ajata (groundmass) composition, and Ra from the contamination of the PAR 011 composition with Belén crust. These recharge magmas are then mixed with the rhyolite composition and finally with the Belén gneiss (contamination after recharge). For all recharge magmas the amount of rhyolite is smaller (20–30%) than in the case of contamination before recharge, and this implies a higher crystal content of the original rhyolite. In any case, the amount of contamination after recharge is at least 20%. This is similar to the entire assimilation seen in the PAR 130 profile and would correspond to the growth of the observed, much smaller, plagioclase calcic rims, implying much faster assimilation in the PAR 082 andesite than in the PAR 130 dacite, possibly related to the higher temperature of the more mafic magma. In summary, post-mixing assimilation appears to be as plausible as pre-mixing assimilation, as discussed above, and the only way to distinguish between the two scenarios is an isotopic investigation of phases recording the earlier history of the recharge magma.

*Depth of crustal assimilation*

Contamination of magmas by crustal assimilation (as discussed for PAR 082 and PAR 068) can happen anywhere between a deep hot zone and the surface (including in the conduit). Different magmas may be formed by contamination of the same parent magma following different ascent paths or at different places in the hot zone. That parent magmas form at different depths in the hot zone is shown by the chemical contrast between the two Ajata magmas: Upper Ajata has higher Sr/Y than Lower Ajata and thorium excess reflecting a garnet signature in the source, and thus a deeper source. However, variations in other Parinacota samples can be related either to the proportions of both magmas (i.e. inherited characteristics) or to the depth and location of further processes. Chemical zoning patterns, in particular patchy zoning, suggest decompression of plagioclase crystals (Nelson & Montana, 1992) in several samples (PAR 082 core, PAR 084 cores, PAR 219 rims), consistent with polybaric evolution of the magmas.

As shown in a previous section, EC-RAFC modelling results for PAR 130 suggest high temperatures for the magma and the country rocks. Higher country-rock temperatures will naturally exist at greater depths. Assuming a $20°C\,km^{-1}$ geotherm, $300°C$ corresponds to 15 km depth (less if the geotherm is hotter), which is in the upper crust (although probably deeper than most upper crustal magma chambers), whereas $600°C$ would correspond to 30 km, which, bearing in mind that the local crust is 70 km thick, is still mid-crust. In fact, the thickness of the crust allows large variations in the temperature of the assimilated wall-rock. Additional preheating may occur if earlier batches of magma have preheated the crust, such as those involved in nearby volcanic centres such as

Caquena, Chucuyo–Vilacollo and Pomerape (5–10 km away from the Parinacota centre), which are between 200 and 300 kyr old (Wörner *et al.*, 2000). Such preheating may be localized laterally or in depth, contributing to a thermally heterogeneous crust.

The temperature of the magmas also affects assimilation by bringing heat into the system. PAR 068 is more mafic than PAR 130, and the repeated recharge events, seen in the multiple crystal dissolution surfaces, suggest more heat in this system. In this case, although mafic recharge and crustal assimilation are competing in terms of Sr concentration and isotope ratios, they are thermally related. As one of the flank eruptions, but slightly higher on the slope of the volcano than Lower and Upper Ajata, High Ajata (PAR 068) may not be part of the main system of magma reservoirs. Magmas here may pass through a dyke system, pond for a short time and be reheated by new hot magma. Enhanced assimilation is thermally favoured by such a configuration (C. Annen, personal communication). This possibility does not necessarily explain why some mafic magmas (PAR 082 and PAR 068) and a (cooler) dacitic magma (PAR 130) show a large amount of assimilation, whereas other mafic magmas (PAR 084) do not. The nature of the crust is also critical for assimilation and probably accounts for some of the variations observed between samples: differences between PAR 084 and Par 068 may be partly explained by differences in the composition of the country rock at the depth of emplacement.

The capacity for the crust to impart isotopic diversity to magmas can be appreciated by considering isotopic variations more regionally. Along the Andean arc samples from the active volcanoes show variations in chemical and isotopic compositions that can be correlated both with crustal thicknesses and with crustal compositions (e.g. Wörner *et al.*, 1992; Mamani *et al.*, 2008). To the east and SE of Parinacota, monogenetic volcanism across the Bolivian Altiplano is isotopically much more diverse (Davidson & de Silva, 1995). Here magmas probably interact with old and variably, but largely deep, crust and ascend to erupt with limited further modification. Similar isotopic and chemical diversity is observed in monogenetic volcanic centers off the main volcanic arc axis in South Peru (Delacour *et al.*, 2007).

At Parinacota, it is only the existence of the associated monogenetic centers (Ajata Cones) that has allowed us to identify (rather than simply infer) distinct magmatic end-members that are identifiable (more or less modified) throughout the entire magma system. At the nearby Pomerape Volcano, only a low-Sr basaltic andesite, similar to Lower Ajata, is erupted at a parasitic vent (Quarter Cone); however, the general geochemical trends of the main cone lavas are indistinguishable from those of Parinacota (Davidson *et al.*, 1990). This suggests that a high-Sr mafic end-member, although not identified in the erupted products, was also present at Pomerape. In fact, despite the complexities described here for Parinacota, the thermal maturation of the crust and the long-term magmatic flux in this locality has rather served to mix and homogenize magmas, resulting in rather limited chemical and isotopic diversity. These kinds of processes are probably typical of central Andean composite volcanoes, and our approach shows how end-member compositions can be teased out from crystal chemical zoning and isotope stratigraphy, even when end-member mafic magmas are not erupted.

## CONCLUSIONS

(1) We have shown how combining isotope and textural *in situ* chemical data can constrain open-system magmatic processes. As in previous isotopic microsampling studies, variations in crystal isotope profiles between and within samples, and evidence for isotopic disequilibrium between crystals and the groundmass in which they are hosted, suggest that many crystals at Parinacota are recycled (antecrysts).

(2) A general negative correlation in drilled zones between Sr concentrations and Sr isotope ratios is consistent with the presence of two distinct mafic magmas. These magmas are similar to those that erupted at flank cinder cones (Ajata), as identified in earlier bulk-rock geochemical studies. In detail, however, the isotopic variations are partly decoupled from the chemical ones, which implies additional and variable contamination of the magmas.

(3) The complexity of both chemical and isotopic zoning patterns in plagioclase crystals, plagioclase populations and, possibly, mineral assemblages, is specific to each sample and reflects the complexity of each magma's history. The more comprehensive the study of both isotopic and chemical zoning in the various crystals and phases is, the more accurately the magma history can be reconstructed. However, the method of interrogating crystals is time consuming and is therefore best used for predefined and focused questions in an otherwise well-known system and in combination with a consistent geochemical and petrological whole-rock dataset.

(4) Single crystal microsampling data can be used to inform complex and sophisticated quantitative models including fractionation, contamination and recharge. We present the first fully quantified model of magma evolution inverted from the core–rim profiles of a single feldspar crystal. In this sample EC-AFC modelling suggests that significant (20%) assimilation occurs in a relatively quiet magma chamber, with one single recharge event recorded, which triggered increased assimilation.

(5) The involvement of significant amounts of crust ($\sim$20%) contrasts with the generally accepted idea that Parinacota, by virtue of its limited range in bulk-rock $^{87}Sr/^{86}Sr$, experienced only limited upper crustal assimilation. It is probably explained by the high Sr concentrations of the magmas and limited isotopic contrast with the crust, which make crustal assimilation not easily detectable.

(6) Local variation of the crust composition and fertility appears to be an important factor controlling variable crustal assimilation. Data are more easily explained if the assimilated crust is either richer in Sr or more radiogenic than the known Belén gneiss basement compositions.

(7) Recharge magmas seem closer to the Ajata end-members in the Healing Flows than in the Old Cone, which is consistent with their ages. It is likely that the end-member mixed in the Young Cone (Healing Flows and Ajata Flows) is the Ajata magmas themselves, whereas in the Old Cone, the recharge magmas are generally either more differentiated or contaminated. It is not clear whether the differences are in the source (evolution of the hot zone over time giving rise to more mafic magmas and a larger diversity in contamination) or in the plumbing system (shorter residence time, different size and geometry).

## SUPPLEMENTARY DATA

Supplementary data for this paper are available at *Journal of Petrology* online.

## REFERENCES

Aitcheson, S. J. & Forrest, A. H. (1994). Quantification of the crustal contamination in open magmatic systems. *Journal of Petrology* **35**, 461–488.

Aitcheson, S. J., Harmon, R. S., Moorbath, S., Schneider, A., Soler, P., Soria-Escalante, E., Steele, G., Swainbank, I. & Wörner, G. (1995). Pb isotopes define basement domains of the Altiplano, Central Andes. *Geology* **23**, 555–558.

Annen, C., Blundy, J. D. & Sparks, R. S. J. (2006). The genesis of calc-alkaline intermediate and silicic magmas in deep crustal hot zones. *Journal of Petrology* **47**, 505–539.

Bacon, C. R. & Hirschmann, M. M. (1988). Mg/Mn partitioning as a test for equilibrium between coexisting Fe–Ti oxides. *American Mineralogist* **73**, 57–61.

Blundy, J. D. & Wood, B. J. (1991). Crystal-chemical controls on the partitioning of Sr and Ba between plagioclase feldspar, silicate melts, and hydrothermal solutions. *Geochimica et Cosmochimica Acta* **55**, 193–209.

Bourdon, B., Wörner, G. & Zindler, A. (2000). U-series evidence for crustal involvement and magma residence times in the petrogenesis of Parinacota volcano, Chile. *Contributions to Mineralogy and Petrology* **139**, 458–469.

Charlier, B. L. A., Ginibre, C., Morgan, D. J., Nowell, G. M., Pearson, D. G., Davidson, J. P. & Ottley, C. J. (2006). Methods for the microsampling and high-precision analysis of strontium and rubidium isotopes at single crystal scale for petrological and geochronological applications. *Chemical Geology* **232**, 114–133.

Clavero, J. E., Sparks, R. S. J., Huppert, H. E. & Dade, W. B. (2002). Geological constraints on the emplacement mechanism of the Parinacota debris avalanche, northern Chile. *Bulletin of Volcanology* **64**, 40–54.

Clavero, J. E., Sparks, R. S. J., Polanco, E. & Pringle, M. S. (2004). Evolution of Parinacota volcano, Central Andes, Northern Chile. *Revista Geologica de Chile* **31**, 317–347.

Davidson, J. P. & de Silva, S. (1995). Late Cenozoic magmatism of the Bolivian Altiplano. *Contributions to Mineralogy and Petrology* **119**, 387–408.

Davidson, J. P. & Tepley, F. J. (1997). Recharge in volcanic systems: evidence from isotope profiles of phenocrysts. *Science* **275**, 826–829.

Davidson, J. P., Harmon, R. S. & Wörner, G. (1991). The source of central Andean magmas: some considerations. In: Harmon, R. S. & Rapela, C. W. (eds) *Andean Magmatism and its Tectonic Setting. Geological Society of America, Special Paper* **265**, 233–243.

Davidson, J. P., MacMillan, N. J., Moorbath, S., Wörner, G., Harmon, R. S. & Lopez-Escobar, L. (1990). The Nevados de Payachata volcanic region (18°S/69°W, N. Chile) II. Evidence for widespread crustal involvement in Andean magmatism. *Contributions to Mineralogy and Petrology* **105**, 412–432.

Davidson, J. P., Morgan, D. J., Charlier, B. L. A., Harlou, R. & Hora, J. M. (2007). Microsampling and isotopic analysis of igneous rocks: implications for the study of magmatic systems. *Annual Review of Earth and Planetary Sciences* **35**, 273–311.

Delacour, A., Gerbe, M.-C., Thouret, J.-C., Wörner, G. & Paquereau-Lebti, P. (2007). Magma evolution of Quaternary minor volcanic centres in Southern Peru, Central Andes. *Bulletin of Volcanology* **69**, 581–608.

Entemann, J. (1994). Magmatic evolution of the Nevados de Payachata complex and the petrogenesis of basaltic andesites in the Central Volcanic Zone of northern Chile. Ph. D. thesis, Johannes Gutenberg-Universität Mainz. 188 pp.

Garrison, J. M., Davidson, J. P., Turner, S. & Reid, M. (2006). Source versus differentiation controls on U-series disequilibria: Insights

from Cotopaxi Volcano, Ecuador. *Earth and Planetary Science Letters* **244**, 548–565.

Ginibre, C. & Wörner, G. (2007). Variable parent magmas and recharge regimes of the Parinacota magma system (N. Chile) revealed by Fe and Sr zoning in plagioclase. *Lithos* **98**, 118–140.

Ginibre, C., Wörner, G. & Kronz, A. (2002). Minor and trace element zoning in plagioclase: implications for magma chamber processes at Parinacota Volcano, N. Chile. *Contributions to Mineralogy and Petrology* **143**, 300–315.

Hammouda, T., Pichavant, M. & Chaussidon, M. (1996). Isotopic equilibration during partial melting: an experimental test of the behaviour of Sr. *Earth and Planetary Science Letters* **144**, 109–121.

Harmon, R. S., Barreiro, B. A., Moorbath, S., Hoeffs, J., Francis, P. W., Thorpe, R. S., Déruelle, B., McHugh, J. & Viglino, J. A. (1984). Regional O-, Sr- and Pb isotope relationships in late Cenozoic calc-alkaline lavas of the Andean cordillera. *Journal of the Geological Society, London* **141**, 803–822.

Hildreth, W. & Moorbath, S. (1988). Crustal contributions to arc magmatism in the Andes of central Chile. *Contributions to Mineralogy and Petrology* **98**, 455–489.

Hora, J., Singer, B. & Wörner, G. (2007). Eruptive flux through thick crust of the Andean central volcanic zone: $^{40}Ar/^{39}Ar$ constraints from Volcan Parinacota, Chile. *Geological Society of America Bulletin* **119**, 343–362.

Hora, J. M., Singer, B. S., Wörner, G., Beard, B. L., Jicha, B. R. & Johnson, C. M. (2009). Shallow and deep crustal control on differentiation of calc-alkaline and tholeiitic magma. *Earth and Planetary Science Letters* **285**, 75–86.

Klemetti, E. W., Deering, C. D., Cooper, K. M. & Roeske, S. M. (2011). Magmatic perturbations in the Okataina Volcanic Complex, New Zealand at thousand-year timescales recorded in single zircon crystals. *Earth and Planetary Science Letters* **305**, 185–194.

Knesel, K. M. & Davidson, J. P. (1996). Isotopic disequilibrium during melting of granite and implication for crustal contamination of magmas. *Geology* **24**, 243–246.

Mamani, M., Tassara, A. & Wörner, G. (2008). Composition and structural control of crustal domains in the central Andes. *Geochemistry, Geophysics, Geosystems* **9**, Q03006, doi:10.1029/2007GC001925.

Martin, V., Davidson, J. P., Morgan, D. & Jerram, D. A. (2010). Using the Sr isotope compositions of feldspars and glass to distinguish magma system components and dynamics. *Geology* **38**, 539–542.

McMillan, N., Davidson, J. P., Wörner, G., Harmon, R. S., Moorbath, S. & Lopez-Escobar, L. (1993). Influence of crustal thickening on arc magmatism: Nevados de Payachata volcanic region, Northern Chile. *Geology* **21**, 467–470.

Morgan, D. J., Jerram, D. A., Chertkoff, D. G., Davidson, J. P., Pearson, D. G., Kronz, A. & Nowell, G. M. (2007). Implications of combined CSD and isotopic microanalysis, the ICSD plot, for understanding magma supply and mixing processes at Stromboli volcano. *Earth and Planetary Science Letters* **260**, 419–431.

Nelson, S. T. & Montana, A. (1992). Sieve-textured plagioclase in volcanic rocks produced by rapid decompression. *American Mineralogist* **77**, 1242–1249.

Sáez, A., Valero-Garcés, B. L., Moreno, A., Bao, R., Pueyo, J. J., González-Sampériz, P., Girat, S., Taberner, C., Herrera, C. & Gilbert, R. O. (2007). Lacustrine sedimentation in active volcanic settings. The Late Quaternary depositional evolution of Lake Chungará (Northern Chile). *Sedimentology* **54**, 1191–1222.

Spera, F. J. & Bohrson, W. A. (2001). Energy-constrained open-system magmatic processes I: General model and Energy-Constrained Assimilation and Fractional Crystallization (EC-AFC) formulation. *Journal of Petrology* **42**, 999–1018.

Spera, F. J. & Bohrson, W. A. (2004). Open-system magma chamber evolution: an energy-constrained geochemical model incorporating the effects of concurrent eruption, recharge, variable assimilation and fractional crystallization (EC-ERAχFC). *Journal of Petrology* **45**, 2459–2480.

Stormer, J. C. (1983). The effects of recalculation on estimates of temperature and oxygen fugacity from analyses of multicomponent iron–titanium-oxides. *American Mineralogist* **68**, 586–594.

Tepley, F. J., Davidson, J. P. & Clynne, M. A. (1999). Magmatic interactions as recorded in plagioclase phenocrysts of Chaos Crags, Lassen Volcanic Center, California. *Journal of Petrology* **4**, 787–806.

Tepley, F. J., Davidson, J. P., Tilling, R. I. & Arth, J. G. (2000). Magma mixing, recharge and eruption histories recorded in plagioclase phenocrysts from El Chichon Volcano, Mexico. *Journal of Petrology* **41**, 1397–1411.

Wallace, G. S. & Bergantz, G.W. (2005). Reconciling heterogeneity in crystal zoning data: an application of shared characteristic diagrams at Chaos Crags, Lassen Volcanic Center, California. *Contributions to Mineralogy and Petrology* **149**, 98–112.

Wörner, G., Harmon, R. S., Davidson, J. P., Moorbath, S., Turner, D. L., McMillan, N., Nye, C., Lopez-Escobar, L. & Moreno, H. (1988). The Nevados de Payachata volcanic region (18°S/69°W, N. Chile): I. Geological, geochemical, and isotopic observations. *Bulletin of Volcanology* **50**, 287–303.

Wörner, G., Moorbath, S. & Harmon, R. S. (1992). Andean Cenozoic volcanic centers reflect basement isotopic domains. *Geology* **20**, 1103–1106.

Wörner, G., Moorbath, S., Horn, S., Entemann, J., Harmon, R. S., Davidson, J. P. & Lopez-Escobar, L. (1994). Large- and fine-scale geochemical variations along the Andean Arc of Northern Chile (17·5°–22°S). In: Reutter, K. J., Scheuber, E. & Wigger, P. J. (eds) *Tectonics of the Southern Central Andes. Structure and Evolution of an Active Continental Margin*. Springer, pp. 77–92.

Wörner, G., Hammerschmidt, K., Henjes-Kunst, F., Lezaun, J. & Wilke, H. (2000). Geochronology ($^{40}Ar/^{39}Ar$, K–Ar, and He-exposure) ages of Cenozoic magmatic rocks from Northern Chile (18°–20°S): Implications for magmatism and tectonic evolution of the central Andes. *Revista Geologica de Chile* **27**, 205–240.